THE ASTROPHYSICAL JOURNAL, 477:313–334, 1997 March 1

EVOLUTION OF HELIUM WHITE DWARFS OF LOW AND INTERMEDIATE MASSES

L. G. ALTHAUS[1] AND O. G. BENVENUTO[2]
Facultad de Ciencias Astronómicas y Geofísicas, Universidad Nacional de La Plata,
Paseo del Bosque S/N, (1900) La Plata, Argentina
Received 1996 May 6; accepted 1996 September 24

ABSTRACT

We present detailed calculations of the evolution of low-mass, helium white dwarf models with masses from $M = 0.1$ to $M = 0.5\ M_\odot$ at intervals of $0.05\ M_\odot$ and with a metallicity of $Z = 10^{-3}$. For this purpose, we have taken fully into account finite-temperature effects by means of a detailed and updated stellar evolutionary code, in which the convective energy transport is described according to the new model for turbulent convection developed by Canuto & Mazzitelli. Furthermore, our code considers the most recent opacity data computed by the Livermore Group (OPAL data), and also the new equation of state for helium plasmas developed by Saumon, Chabrier, & Van Horn. Neutrino emission is fully taken into account as well.

For models with $M \leq 0.3\ M_\odot$ we started our calculations from fully convective models located at the helium-Hayashi line for each configuration, far away from the white dwarf regime. By contrast, the evolutionary sequences corresponding to 0.35, 0.4, 0.45, and $0.5\ M_\odot$ were started from initial models resembling white dwarf structures. This was necessary in order to avoid the onset of helium burning. A consequence of this constraint is the existence of a "forbidden region" in the HR diagram above $\log (L/L_\odot) = -0.25$ and hotter than $\log T_{\rm eff} = 4.45$, where helium white dwarfs can exist only for brief intervals. All the models were evolved to $\log (L/L_\odot) = -5$.

The evolutionary tracks in the HR diagram have been carefully analyzed, and we found that the convective efficiency affects the tracks noticeably only in the high-luminosity (pre–white dwarf) regime. We also examined the evolution of central conditions, neutrino luminosity, radii, surface gravity, and ages. Central densities, radii, and surface gravities asymptotically approach the zero temperature Hamada-Salpeter results, as expected. Neutrino losses are important for the more massive helium white dwarf configurations and should be taken into account in detailed evolutionary studies of these objects.

Finally, the structure of the outer convective zone was analyzed in both the framework of the mixing length theory (for different convective efficiencies) and the Canuto & Mazzitelli theory. We found that the profile of the outer convective zone given by the Canuto & Mazzitelli model is very different from that given by any version of the mixing length theory. This behavior is critical for pulsational instability; however, stellar parameters such as radius and surface gravity are not significantly affected in the white dwarf domain.

These models should be especially suitable for the interpretation of the data about the recently discovered low-mass white dwarfs in systems containing another white dwarf or a millisecond pulsar.

Subject headings: pulsars: general — stars: evolution — stars: interiors — white dwarfs

1. INTRODUCTION

It is now widely accepted that helium white dwarf (He WD) stars cannot be the result of the evolution of single stars within the lifetime of our Galaxy but, on the contrary, they should have their origin in the evolution of close binary systems. Here, He WDs would be formed through a chain of events radically different than that expected for WDs coming from single progenitors of the initial main sequence (for details, see, e.g., Iben & Webbink 1989; de Kool & Ritter 1993; Iben & Tutukov 1993). In view of these considerations, the existence of He WDs with masses as low as $0.1\ M_\odot$ should be feasible, something that would be impossible for single-star progenitors, at least in a Hubble time. He WDs would be the final product of the evolution of some close binary systems provided the first Roche lobe overflow phase occurs prior to helium ignition in the primary star.

The contribution of such binary systems to the observed DA WD mass distribution has been discussed by Bergeron, Saffer, & Liebert (1992) and more recently by Bragaglia, Renzini, & Bergeron (1995). According to these authors, the mass distribution exhibits a more extended tail at low masses than found in earlier investigations. More precisely, they concluded that nearly 10% of presently known DA WDs have masses low enough that they are the product of close binary system evolution.

Very recently, careful observations of seven previously considered low-mass ($M < 0.45\ M_\odot$) single WDs revealed that five of them are indeed detached close binary systems for which the most probable configuration is a pair of WDs (Marsh, Dhillon, & Duck 1995). Moreover, Marsh (1995) has discovered a binary WD system with an orbital period of 4 hr, which will merge (due to gravitational radiation) in $\approx 2 \times 10^9$ yr.

Another astrophysical system in which we may expect He WDs is in binary systems in which the companion is a millisecond pulsar. Very recently, Lundgren et al. (1996) detected two of these systems and studied properties of these pulsars considering data about the WD. The study of these systems may also provide clues for understanding

[1] Fellow of the Consejo Nacional de Investigaciones Científicas y Técnicas (CONICET), Argentina; althaus@fcaglp.fcaglp.unlp.edu.ar.
[2] Member of the Carrera del Investigador Científico, Comisión de Investigaciones Científicas de la Provincia de Buenos Aires (CIC), Argentina; obenvenuto@fcaglp.fcaglp.unlp.edu.ar.

magnetic field decay in neutron stars, the cooling of WDs, etc. Previous to the work cited above, only three WD-pulsar systems were known, and two of them have non-millisecond pulsars (see Lundgren et al. 1996, and references therein).

Other objects involving low-mass WDs are Feige 24 (Vennes & Thorstensen 1994) and the detached WD/M dwarf system detected by Marsh & Duck (1996). In both systems the WD component is suspected to be a He WD.

All this observational evidence clearly favors low-mass WDs being the result of close binary system evolution. Moreover, such systems may be used to impose constraints upon the ejection of the common envelope. Since the theoretical computation of the common envelope stage is difficult, observational data is particularly desirable (Marsh et al. 1995).

Numerical models of close binary degenerate dwarfs indicate that the majority of WDs in close binaries would be composed by helium. In particular, Iben, Tutukov, & Yungelson (1996) applied a numerical scenario code to construct a model of the population of young WDs in close binaries with an older WD companion or a low-mass (≤ 0.3 $M_{\odot}$) main-sequence companion. They found that in the 82% of the systems that consist of two close WDs, the brighter component is a He WD. This accounts for the fact that the majority of WDs discovered to date in close binary systems are He WDs.

It is clear that, in order to make an adequate interpretation of observational data, we need models of He WDs as accurate and detailed as possible. However, in spite of the above facts, little attention has been paid to the study of He WDs. The early works on this topic have been those of D'Antona, Magni, & Mazzitelli (1972) and Chin & Stothers (1971). Much more recently, Nelson, Joss, & Rappaport (1989) presented computations of the cooling of He WDs for objects with 0.05, 0.1, and 0.15 $M_{\odot}$ but with emphasis on the phenomenology of the X-ray burster 4U 1820−30. To our knowledge, no further attempt to compute the evolution of low-mass He WDs has, so far, been carried out.

Vennes, Fontaine, & Brassard (1995) have presented static mass-radius relations for He WDs in the range of high effective temperatures ($T_{\rm eff}$) in order to apply them to the interpretation of some observed objects. However, they neglected neutrino emission and assumed a constant luminosity-to-mass ratio in the interior, which is not a good assumption for their hottest models.

By contrast, the structure and evolution of the outer convective zone (OCZ) in carbon-oxygen WDs with hydrogen- and helium-rich outer layers (DA and DB types, respectively) have been analyzed in a large number of investigations, such as those performed by Fontaine & Van Horn (1976), D'Antona & Mazzitelli (1979), Winget et al. (1982), Winget et al. (1983), Tassoul, Fontaine, & Winget (1990), D'Antona & Mazzitelli (1990), Fontaine & Wesemael (1991), Bradley & Winget (1994), and references therein. Such large interest is motivated because of the key role played by convection both in pulsating WDs and in the chemical evolution that occurs in the outer layers of DA WDs through mixing episodes. These studies have shown, in particular, that the thickness (in the Lagrangian coordinate) of the OCZ as WDs pass through instability strips can differ by several orders of magnitude according to the assumed convective efficiency. This strong sensitivity to the convective efficiency has made it possible to adjust the free parameters involved in the mixing-length theory (MLT) (Böhm-Vitense 1958) in the context of WD envelopes. It is worth noting that in the works cited above, the authors only use variations of MLT.

A more realistic approach to the treatment of turbulent convection in stars has been presented by Canuto & Mazzitelli (CM) (1991, 1992). The convection theory developed by these authors does not have parameters that must be calibrated and represents a considerable improvement with respect to the MLT. Unlike the MLT treatment in which the spectrum of turbulent eddies is represented by a single, large eddy, the CM theory (CMT) takes into account the whole spectrum of eddy sizes by using modern theories of turbulence. This becomes relevant in the case of the nearly inviscid fluids present in stellar interiors for which the MLT is not a completely satisfactory approach. In fact, CM have shown that their model provides, at high convective efficiency, a turbulent flux up to ≈ 10 times larger than that of the MLT. It is worth mentioning that the CMT has been successfully tested in different stellar objects; see, e.g., D'Antona, Mazzitelli, & Gratton (1992), Paternò et al. (1993), D'Antona & Mazzitelli (1994), and Stothers & Chin (1995). In the case of our Sun, employing the CMT, its $T_{\rm eff}$ is fitted within 0.5% of the observed value *without free parameters*. Concerning WDs, Althaus & Benvenuto (1996) (see also Mazzitelli & D'Antona 1991) have applied the CMT to the study of the OCZ of carbon-oxygen WDs with He envelopes and masses covering the observed WD mass distribution. Althaus & Benvenuto (1996) use thermal timescale arguments to show that the CMT predicts blue edges for the DB WD instability strip in good agreement with observations (Thejll, Vennes, & Shipman 1991).

We have two main motivations for this study. On the one hand, there is increasing observational evidence that low- and intermediate-mass He WDs correspond to a substantial class of observed objects. On the other hand, there are no recent detailed computations of the structure and evolution of He WDs capable to provide a reference frame solid enough to allow for a good interpretation of the collected data on WDs in the referenced observational works.

For this purpose, we evolved He WD models with masses ranging from 0.1 to 0.5 $M_{\odot}$ with steps of 0.05 $M_{\odot}$ for low and intermediate $T_{\rm eff}$ employing both the CMT and the MLT of convection. The calculations were carried out by means of a full stellar evolutionary code developed by us in which, chiefly, new OPAL radiative opacities (Rogers & Iglesias 1994) and the equation of state for helium composition developed by Saumon, Chabrier, & Van Horn (1995) were considered. Also neutrino energy losses were included. Such a description becomes necessary if accurate mass and radius determinations for WDs are required. In this context, we shall show that the radii and surface gravities of our evolutionary models and those predicted by Hamada & Salpeter (1961, hereafter H-S) for zero-temperature, degenerate configurations differ significantly, especially in the case of low-mass models (see also Koester & Schönberner 1986 for the case of carbon-oxygen WDs).

The remainder of this paper is organized as follows. We begin in § 2 by giving a general description of the main improvements of the new CMT with respect to the MLT and also, we comment on the equation of state, radiative and conductive opacities, and neutrino emission processes included in our code. Next, in § 3 we present a brief description of the main features of our evolutionary code, particu-

larly those concerning to the outer layer integration. Then, we address the crucial problem of the initial models in § 4. Section 5 is devoted to presenting and analyzing our results and, finally, § 6 summarizes our findings.

2. INPUT PHYSICS

2.1. *Convection Theories*

Because of the fundamental role played by convection in determining both the thermal structure and surface composition (through possible mixing episodes) of the outer layers of WDs and their pulsational properties as well, the complex nature of the convective processes occurring in such stars should be fully taken into account. An extremely simplified representation of such convective processes is provided by the MLT. This convection theory, which has been employed in most of the relevant WD calculations, contains three free parameters usually reduced, in stellar studies, to a single one: the *mixing length* traveled by the convective eddies, parameterized as a fraction of the local pressure scale height H_p, $l = \alpha H_p$ (see Cox & Giuli 1968 for details). Concerning WDs, the free parameter α is usually adjusted from observations of pulsating WDs (see Tassoul et al. 1990; Koester, Allard, & Vauclair 1994; Bradley & Winget 1994, and references therein). However, the most drastic approximation assumed in the MLT is the representation of the full spectrum of eddy sizes by means of single-size, large eddies, which constitutes a poor description of convection in stellar interiors. Such representation is justified only for very viscous flows, for which the spectrum of eddy sizes is extremely reduced. But a stellar interior is a nearly inviscid environment, so that the entire spectrum must be taken into account in order to compute the actual convective energy flux accurately (see CM).

By contrast, in their convection theory, CM computed the whole spectrum of turbulent eddies by using modern theories of turbulence, where the size ratio of the largest to the smallest eddy is $\gtrsim 10^6$. Specifically, CM fitted their values for the convective flux (proportional to Φ) as

$$\Phi = \left(\frac{K_0}{1.5}\right)^3 a_1 \Sigma^m [(1 + a_2 \Sigma)^n - 1]^p , \quad (1)$$

where K_0 is the Kolmogorov constant and the coefficients are given by $a_1 = 24.868$, $a_2 = 9.7666 \times 10^{-2}$, $m = 0.14972$, $n = 0.18931$, and $p = 1.8503$. Σ is a measure of the convective efficiency and is defined as

$$\Sigma \equiv 4A^2(\nabla_{\rm conv} - \nabla_{\rm ad}) , \quad (2)$$

where $\nabla_{\rm conv}$ and $\nabla_{\rm ad}$ are the convective and adiabatic temperature gradient, respectively, and A is given by

$$A = \frac{c_p \rho^2 \kappa z^2}{12acT^3} \left(\frac{g\delta}{2H_p}\right)^{1/2} , \quad (3)$$

where z is the mixing length (see below), and the other quantities have their usual meaning (see CM for further details). CM assume $K_0 = 1.5$; we instead elect to adopt $K_0 = 1.8$ (Mazzitelli 1994).

In the standard MLT of Böhm-Vitense (1958), the parameters of equation (1) have the values $a_1 = 9/8$, $a_2 = 1$, $m = -1$, $n = \frac{1}{2}$, and $p = 3$. For large convective efficiencies (large values of Σ), $\Phi_{\rm CM} \approx 10\Phi_{\rm MLT}$, which will have its greatest impact on the temperature stratification in those non-adiabatic regions where the radiative opacity κ is relatively high (the superadiabatic transition region).

Another improvement of the CMT is that this theory does not have parameters that must be calibrated. In fact, CM put forward that the mixing length be taken as $l = z$, where z is the distance from the top of the convection zone to the point at which $\nabla_{\rm conv}$ is computed.

2.2. *The Equation of State*

In the present work, we used the new equation of state (EOS) presented by Saumon et al. (1995), which provides a detailed description of the thermodynamics of matter inside low-mass stars and giant planets. Since this EOS does not cover the whole temperature-density regime characterizing most of the objects in which we are interested, it was complemented by other EOSs. More specifically, the Saumon et al. EOS was used in the low-density and low-temperature regime limited by $4 < \log P < 19$ and by $\log T < 7$, where P is given in ergs cm^{-3} and T in K. Though the main emphasis of Saumon et al. (1995) is on the EOS of a pure hydrogen plasma and their treatment of a helium plasma is not so detailed, it is the best EOS available at present. Outside the range covered by this EOS, we employed an updated version (Mazzitelli 1993) of the Magni & Mazzitelli (1979) EOS. We use this EOS up to $\rho \approx 2 \times 10^3$ g cm^{-3}. For higher densities, we adopted the treatment described below (see also Benvenuto & Althaus 1995). At such conditions we considered an ideal gas plus radiation pressure, subject to Coulomb interactions, and quantum corrections for the ions as described by Hansen (1973). Fermi-Dirac integrals for partially degenerate electrons were calculated according to Kippenhahn & Thomas (1964) for strong and weak degeneracy. Likewise, electron exchange and Thomas-Fermi contributions at finite temperature were included following the procedure given by Shaviv & Kovetz (1972) and Kovetz, Lamb, & Van Horn (1972) (see Appendix for details).

Unlike carbon-oxygen WDs, which at some stage of their evolution undergo core crystallization, He WDs never reach such a state of internal crystallization at least in the range of stellar masses and luminosities covered by our study (see, e.g., Van Horn 1968). This is a consequence of the relatively weak Coulomb interactions between helium nuclei.

2.3. *Radiative and Conductive Opacities*

In our study we have included two different sets of radiative opacities. For the regime of $T \geq 6000$ K we considered the latest OPAL (Iglesias & Rogers 1993) radiative opacities and for $T < 6000$ K we included the old data of Cox & Stewart (1970). We have allowed for a low metal abundance Z by adopting $Z = 10^{-3}$. The reason for this choice is that this is the lowest nonzero value of Z existing in both sets of tables. The effect of varying the values of Z on the high $T_{\rm eff}$ models will be explored in a future study.

The OPAL data represents a large improvement compared to earlier radiative opacity calculations. Such improvements are due to a more detailed treatment of atomic models (see Rogers & Iglesias 1994). In most of the astrophysically interesting conditions, it was found that the radiative opacity was (in some cases largely) underestimated and that the exact value is strongly dependent upon the iron content of the plasma. Such data provided better agreement of stellar models with observations in problems like helioseismology and stellar pulsations in general, lithium deple-

tion, red supergiants structure, etc. (see Rogers & Iglesias 1994 for details).

In the case of $T < 6000$ K (not covered by OPAL data) we have had to employ the old tabulation of Cox & Stewart (1970). To our knowledge, a more recent computation of radiative opacities for a *helium-dominated* plasma at low temperatures and with a heavy element content compatible with OPAL data is not presently available. This is the main reason for our choice.

It is also worth mentioning that we studied the possibility of including more recent tables from Huebner et al. (1977). However, we decided not to employ them because the opacity values for hydrogen-free composition of $Z = 10^{-3}$ are, by far, larger than the Cox & Stewart (1970) data (see also D'Antona & Mazzitelli 1990) and especially with respect to OPAL data at the temperatures and densities with overlapping data.

The OPAL data covers low and intermediate densities, so that they cover most of the conditions attained at the interior of low-mass ($M \lesssim 0.3\ M_\odot$) He WDs. However, for more massive WDs, some required values are lacking. In particular, at high $T_{\rm eff}$, the most massive model we consider ($M = 0.5\ M_\odot$) lies within the opacity table boundaries, except for very high densities where opacity contribution is dominated by degenerate electrons. When $T_{\rm eff} \leq 15{,}000$ K, the density in the outer layers is so high that we do not have radiative opacity information from any table. Therefore, we extrapolated, at constant temperature, the values of opacity of the mentioned tables to the high-density regime. This imprecise (but unavoidable) procedure is not as bad as it sounds, because (as pointed out by Fontaine & Van Horn 1976) a detailed knowledge of radiative opacities at low $T_{\rm eff}$ is unnecessary in most of the OCZ (except in the atmosphere) because of the nearly adiabatic character of the convection zone. In the context of our present discussion, our lowest luminosity models are intended as a guide, because their physics are less reliable than for hotter models.

As far as conductive opacities are concerned, we used the analytic fits given by Fontaine & Van Horn (1976). These fits, which are based on calculations of conductive opacities of Hubbard & Lampe (1969), were considered for values of the plasma coupling constant $\Gamma \leq 2$ (expressed, for helium composition, as $\Gamma = 5.719 \times 10^5 \rho^{1/3}/T$) ; for higher values of Γ (liquid phase) we follow the treatment given by Itoh et al. (1983).

2.4. *Neutrino Emission*

Neutrino energy losses represent the dominant contribution to the cooling during the hot phases of WD evolution, and their effect should be taken into account at least for the more massive models. We have, therefore, included in our models the main neutrino processes according to the formulation of Itoh and collaborators. Specifically, pair and photo neutrino have been taken from Itoh et al. (1989, see also erratum); plasma neutrino from Itoh et al. (1989) and from Itoh et al. (1992, see also erratum) for strongly degenerate electrons. Neutrino Bremsstrahlung were included from the works of Itoh & Kohyama (1983) for the liquid phase and from Munakata, Kohyama, & Itoh (1987) for partially degenerate electrons.

3. EVOLUTIONARY CODE

In this section, we comment on some general characteristics of our evolutionary code. This code has been written independently of other researchers (Benvenuto 1988) following the method of triangles to derive the surface boundary conditions as described in Kippenhahn, Weigert, & Hofmeister (1967). The atmosphere has been integrated in the gray approximation so that the constancy of radiative flux is satisfied at each point in the atmosphere according to the Unsöld procedure (see Mihalas 1970). To this end, the equations of hydrostatic equilibrium and continuity are solved via a Runge-Kutta method in terms of the optical depth τ. The starting values τ_0 and P_0 at the top of the atmosphere are found by means of an iterative procedure from a initial value of the density, which is assumed to be $\rho \approx 10^{-8}$ g cm^{-3}. The atmospheric integration proceeds inward to the point where convection, according to the Schwarzschild criterion, sets in (or to $\tau = \frac{2}{3}$ if convection is absent), and the final values corresponding to $P_{\rm atm}$, $r_{\rm atm}$ (radial distance), $T_{\rm atm}$, and $q_{\rm atm}$ (with $q = M_e/M_*$, where M_e is the external mass and M_* is the total mass of the model) are then used to start the integration of the four stellar interior equations, taking now as independent variable the total pressure P and assuming a constant luminosity (envelope integration). This method of integration is essentially the one employed by Fontaine & Van Horn (1976), though these authors extended the atmosphere to $\tau \approx 10$. The calculations are pursued inward to a fitting mass fraction q_F corresponding to the first Henyey mass shell. The thickness of the envelope is always kept small enough so the constancy of the luminosity assumed in the envelope remains valid. Naturally, in the course of evolution, $q_{\rm atm}$ varies as a result of changes in the surface opacities. If the atmosphere becomes so thick that $q_{\rm atm}$ is located beyond the prescribed fitting shell ($q_{\rm atm} > q_F$), we changed q_F by taking $q_F = 1.15\ q_{\rm atm}$ as a new value. Also, if the atmosphere becomes thinner (for instance, with low-mass models during the pre-WD stages), we inserted new mesh points in order to get an accurate description of these layers.

It is worth noting that, in the case of convective envelopes, the top of the OCZ is located near the photosphere ($\tau = \frac{2}{3}$; see § 5); accordingly the diffusion approximation assumed even in the most external part of the envelope remains valid. Finally, the interior integration was treated according to the standard Henyey technique as described in Kippenhahn et al. (1967).

We describe now some details that were necessary to take into account in order to implement the CMT in our evolutionary code, particularly those concerning the numerical convergence of the models. Because of the fact that in the CMT the mixing length is taken as $l = z$ and considering that the superadiabatic transition region in WDs is restricted exclusively to an extremely narrow range of r, a careful treatment of this coordinate becomes absolutely indispensable. To this end, our models were divided into approximately 2000 mesh points, most of them distributed in the outer layers, and more importantly, the size of the triangles in the HR diagram were assumed to be very small ($\Delta \log T_{\rm eff} = 2 \times 10^{-4}$ and $\Delta \log L = 10^{-3}$).[3] Such small triangles are necessary in order to avoid having strong discontinuities in the convective gradient $\nabla_{\rm conv}$ at q_F. In fact, a tiny difference between the value of r at the bottom of the

[3] Note, however, that in the pre-WD stages, the OCZ may be very deep. In such cases, we had to employ somewhat larger triangles in order to avoid numerical difficulties.

envelope and at q_F would lead to changes of z of several orders of magnitude (because $z \ll r$ in all the OCZ) and, accordingly, to a discontinuity in $\nabla_{\rm conv}$. More specifically, in each of the three envelope integrations necessary to specify the surface boundary conditions, we determine the location (in r) of the top of the OCZ (z_0) from where z is measured.[4] After the three envelope integrations, the location of the top of the OCZ is obtained through the usual interpolation in the Kippenhahn et al. (1967) triangles of the three values of z_0.

Concerning the computation of $\nabla_{\rm conv}$, we proceed as follows. From the expression of $\Phi_{\rm CM}$, equation (1), $\nabla_{\rm conv}$ can be easily computed by means of a simple iterative procedure. For the sake of simplicity, we have built, as suggested by CM, a three-dimensional table, from which $\log (\nabla_{\rm conv} - \nabla_{\rm ad})$ can be found through interpolation as a function of $\log (\nabla_r - \nabla_{\rm ad})$ and $\log A$ (eq. [3]), where ∇_r is the radiative gradient.

4. INITIAL MODELS

We used an artificial procedure to generate our initial models of different masses starting from a 0.55 $M_\odot$ carbon-oxygen WD model kindly provided to us by Prof. Franca D'Antona. This method is a bit different from what we previously employed (Benvenuto & Althaus 1995). In order to get a helium model of a given mass, we artificially changed the mass and chemical composition of the D'Antona's model in steps of $\sim$20%. Also, in order to produce a luminous enough model, we added an artificial energy release of the form $\varepsilon_{\rm artif} = CT^n$, where $\varepsilon_{\rm artif}$ is the artificial energy release per gram and second, C and n are constants, and T is the temperature. Initially, we took $n = 1$ (fixed) and C small enough to guarantee convergence, and then we increased its value, typically in steps of 25%. With this procedure, we produce helium star models on the corresponding helium-Hayashi line. When the model reached $\log (L/L_\odot) \gtrsim 2$, we started to switch C off smoothly, reaching a structure without any transitory (due to this artificial procedure) in few tens of models.

We have adopted these initial models because it is our interest to perform this study under the most general conditions. Binary evolution could produce helium objects with a wide variety of structures. Nevertheless, such structures should asymptotically reach our evolutionary tracks. Obviously, our starter model choice strongly affects the initial evolution of the objects, but this transient behavior damps out fairly quickly and is not noticeable in faint models.

In this context, it is worth mentioning that Iben & Tutukov (1993, see other references cited therein) calculated the evolution of close binary systems for different initial conditions. They found that binary components with initial masses less than $\approx$2.3 $M_\odot$ may eventually become He WDs, provided the Roche-lobe filling occurs before the helium flash in the primary component. In particular, after the common-envelope event, the $\approx$0.3 $M_\odot$ remnant (see Fig. 1 in Iben & Tutukov 1993) ultimately reaches our corresponding track at $\log (L/L_\odot) \approx 0.2$.

Our less massive models ($M \leq 0.30\ M_\odot$) do not reach temperatures high enough for helium burning reactions to be ignited in their interiors, and so, the evolution has been considered starting from models on the Hayashi line. More massive models starting from this initial condition would burn helium and would not form a He WD. Thus, we considered the evolution during the high central temperature conditions, neglecting the effects of the 3α reaction on the structure, and considered as plausible an initial model that fulfills the condition that $L_{\rm nuclear}/L \lesssim 10^{-3}$. As consequence of this key constraint on the initial models, we found a forbidden region in the HR diagram above $\log (L/L_\odot) = -0.25$ and hotter than $\log T_{\rm eff} = 4.45$, where He WDs can exist only for brief intervals. At somewhat higher $T_{\rm eff}$, the value of the central temperature in these massive models would be so high that helium would ignite under degenerate conditions, preventing the formation of a He WD. In this context, it is worth repeating that all of our models should be regarded as evolutionary stages that may be reached *asymptotically* as a product of the evolution of binary systems. In this sense, a proto-He WD could evolve through the forbidden region, but this phase will last for a very short time. This is because such an object should have hotter outer layers and an interior cooler than predicted by our equilibrium models, enforcing a fast evolutionary situation. In particular, after the common envelope phase, the helium degenerate remnants of $\approx$0.3 and 0.4 $M_\odot$ calculated by Iben & Tutukov (1993) evolve through the forbidden region and rapidly reach our tracks at $\log (L/L_\odot) < 0$.

We have calculated the zero-age main sequence (ZAMS) of helium stars under the usual approximation of neglecting the temporal derivative of the entropy in the luminosity equation. This approximation is the same as that employed in creating a ZAMS model for the Sun. In doing so, we incorporated in our code the 3α energy release given by Kippenhahn & Weigert (1990) and electron screening following Wallace, Woosley, & Weaver (1982). We found stable models corresponding to these conditions for stars up to $\approx$0.29 $M_\odot$. This is in contrast to our full computations that indicate that only objects with $M \gtrsim 0.31\ M_\odot$ actually ignite helium in the core (see below). This rather paradoxical behavior is because the temporal derivative of the entropy has a *non*-negligible effect on the evolution of these stars, and so, our *evolutionary* models are the correct ones.

Let us comment that we have also performed the artificial heating procedure choosing $n = 0.8$ for constructing the initial models. The results we found in this case converge to the case of $n = 1$ in a number of models much smaller than that necessary for the transient behavior to vanish. This is a good indication that our models are indeed well behaved.

In this attempt to compute the structure and cooling of He WDs in the CMT, we have not taken into consideration a possible thin, outer hydrogen envelope (see, e.g., Iben & Webbink 1989). The effect of a hydrogen layer in our models will be considered in a future paper.

5. EVOLUTIONARY RESULTS

5.1. *General Characteristics*

In view of the lack of modern extensive computations of the evolution of He WDs that can offer a good interpretation to the observations of low-mass WD objects (Bergeron et al. 1992; Bragaglia et al. 1995; Lundgren et al. 1996), one of the aims of the present work has been to fill this gap with realistic evolutionary models. In this section, we present the results of our calculations for He WD configurations with

[4] To avoid numerical difficulties, we add to z_0 a negligible overshooting, which is taken as a small fraction ($\approx$0.1) of H_p. We checked, and such overshooting has no influence on the convective stratification.

TABLE 1

SELECTED STAGES FOR A 0.10 $M_\odot$ HELIUM WHITE DWARF

log $L/L_\odot$	log $L_\nu/L_\odot$	log $T_{\rm eff}$	log T_c	log ρ_c	log g	log $R/R_\odot$	log (Age)
1.000	< -6.00	4.003	6.247	-0.047	3.404	0.017	$-\infty$
0.900	< -6.00	4.007	6.300	0.117	3.522	-0.042	3.731
0.800	< -6.00	4.012	6.350	0.275	3.639	-0.101	3.921
0.700	< -6.00	4.015	6.402	0.438	3.754	-0.158	4.105
0.600	< -6.00	4.019	6.455	0.600	3.868	-0.215	4.276
0.500	< -6.00	4.021	6.507	0.759	3.979	-0.271	4.436
0.400	< -6.00	4.024	6.558	0.916	4.088	-0.325	4.591
0.300	< -6.00	4.025	6.608	1.070	4.195	-0.379	4.739
0.200	< -6.00	4.026	6.658	1.221	4.298	-0.430	4.883
0.100	< -6.00	4.027	6.706	1.369	4.399	-0.481	5.028
0.000	< -6.00	4.026	6.753	1.515	4.498	-0.530	5.170
-0.100.....	< -6.00	4.025	6.798	1.654	4.593	-0.578	5.308
-0.200.....	< -6.00	4.023	6.842	1.790	4.684	-0.623	5.444
-0.300.....	< -6.00	4.020	6.883	1.918	4.772	-0.667	5.576
-0.400.....	< -6.00	4.015	6.921	2.040	4.854	-0.708	5.703
-0.500.....	< -6.00	4.010	6.958	2.155	4.933	-0.748	5.828
-0.600.....	< -6.00	4.003	6.992	2.265	5.007	-0.785	5.951
-0.700.....	< -6.00	3.996	7.024	2.370	5.077	-0.820	6.072
-0.800.....	< -6.00	3.988	7.055	2.471	5.146	-0.854	6.195
-0.900.....	< -6.00	3.979	7.083	2.557	5.210	-0.886	6.312
-1.000.....	< -6.00	3.969	7.107	2.649	5.269	-0.916	6.427
-1.100.....	< -6.00	3.958	7.128	2.736	5.326	-0.944	6.540
-1.200.....	< -6.00	3.946	7.146	2.821	5.378	-0.970	6.650
-1.300.....	< -6.00	3.934	7.162	2.905	5.428	-0.995	6.760
-1.400.....	< -6.00	3.921	7.176	2.990	5.476	-1.019	6.871
-1.500.....	< -6.00	3.908	7.190	3.079	5.524	-1.043	6.987
-1.600.....	< -6.00	3.895	7.203	3.173	5.571	-1.067	7.110
-1.700.....	< -6.00	3.882	7.217	3.278	5.622	-1.092	7.242
-1.800.....	< -6.00	3.873	7.236	3.419	5.685	-1.124	7.409
-1.900.....	< -6.00	3.866	7.256	3.570	5.757	-1.160	7.586
-2.000.....	< -6.00	3.861	7.276	3.730	5.837	-1.200	7.767
-2.100.....	< -6.00	3.856	7.289	3.874	5.915	-1.239	7.929
-2.200.....	< -6.00	3.848	7.292	3.985	5.983	-1.273	8.060
-2.300.....	< -6.00	3.838	7.288	4.093	6.045	-1.304	8.177
-2.400.....	< -6.00	3.828	7.275	4.180	6.106	-1.334	8.292
-2.500.....	-5.983	3.816	7.252	4.247	6.156	-1.359	8.397
-2.600.....	-5.963	3.803	7.226	4.313	6.205	-1.384	8.504
-2.700.....	-5.985	3.789	7.196	4.367	6.248	-1.405	8.601
-2.800.....	< -6.00	3.772	7.163	4.405	6.281	-1.422	8.684
-2.900.....	< -6.00	3.754	7.129	4.439	6.309	-1.436	8.763
-3.000.....	< -6.00	3.737	7.092	4.471	6.340	-1.451	8.843
-3.100.....	< -6.00	3.719	7.055	4.499	6.369	-1.466	8.921
-3.200.....	< -6.00	3.701	7.014	4.524	6.398	-1.480	8.996
-3.300.....	< -6.00	3.683	6.972	4.546	6.426	-1.494	9.070
-3.400.....	< -6.00	3.665	6.927	4.566	6.451	-1.507	9.139
-3.500.....	< -6.00	3.645	6.878	4.583	6.473	-1.518	9.208
-3.600.....	< -6.00	3.625	6.828	4.598	6.493	-1.528	9.274
-3.700.....	< -6.00	3.604	6.776	4.612	6.509	-1.536	9.338
-3.800.....	< -6.00	3.583	6.722	4.624	6.524	-1.543	9.400
-3.900.....	< -6.00	3.561	6.665	4.634	6.537	-1.550	9.462
-4.000.....	< -6.00	3.539	6.605	4.643	6.550	-1.556	9.523
-4.100.....	< -6.00	3.517	6.538	4.652	6.562	-1.562	9.586
-4.200.....	< -6.00	3.495	6.474	4.659	6.574	-1.568	9.643
-4.300.....	< -6.00	3.473	6.405	4.665	6.585	-1.574	9.699
-4.400.....	< -6.00	3.450	6.337	4.671	6.594	-1.578	9.753
-4.500.....	< -6.00	3.427	6.266	4.675	6.601	-1.582	9.804
-4.600.....	< -6.00	3.404	6.194	4.679	6.607	-1.585	9.854
-4.700.....	< -6.00	3.380	6.121	4.682	6.612	-1.587	9.903
-4.800.....	< -6.00	3.356	6.043	4.685	6.616	-1.589	9.952
-4.900.....	< -6.00	3.332	5.966	4.688	6.620	-1.591	9.999
-5.000.....	< -6.00	3.308	5.886	4.690	6.623	-1.593	10.046

masses ranging from $M = 0.1\ M_\odot$ to $M = 0.5\ M_\odot$ at intervals of $0.05\ M_\odot$ and a metallicity of $Z = 10^{-3}$. These models were evolved through the phases of increasing internal degeneracy to $\log (L/L_\odot) = -5$, where we stopped the calculations.

As pointed out in the foregoing section, except for the more massive models, we started our calculations from fully convective initial models located in the neighborhood of what we regard as the helium-Hayashi line for each configuration. Needless to say, such models are not representative of WD structures, but they relax to degenerate configurations. By contrast, the evolutionary sequences corresponding to 0.35, 0.4, 0.45, and $0.5\ M_\odot$ were started from initial models resembling WD structures. As mentioned before, this choice was dictated by the fact that more massive models are characterized by higher internal tem-

TABLE 2

SELECTED STAGES FOR A 0.15 $M_\odot$ HELIUM WHITE DWARF

log $L/L_\odot$	log $L_w/L_\odot$	log $T_{\rm eff}$	log T_c	log ρ_c	log g	log $R/R_\odot$	log (Age)
1.000	<-6.00	4.020	6.436	0.198	3.648	−0.017	$-\infty$
0.900	<-6.00	4.025	6.491	0.366	3.767	−0.077	4.073
0.800	<-6.00	4.030	6.547	0.539	3.887	−0.137	4.285
0.700	<-6.00	4.034	6.603	0.707	4.003	−0.195	4.461
0.600	<-6.00	4.037	6.657	0.870	4.116	−0.251	4.639
0.500	<-6.00	4.041	6.713	1.040	4.232	−0.309	4.802
0.400	<-6.00	4.043	6.765	1.198	4.340	−0.363	4.954
0.300	<-6.00	4.043	6.814	1.348	4.442	−0.414	5.097
0.200	<-6.00	4.044	6.865	1.502	4.547	−0.467	5.251
0.100	<-6.00	4.046	6.916	1.660	4.654	−0.520	5.398
0.000	<-6.00	4.049	6.970	1.823	4.764	−0.575	5.556
−0.100.....	<-6.00	4.049	7.017	1.971	4.863	−0.625	5.706
−0.200.....	<-6.00	4.044	7.056	2.095	4.947	−0.666	5.827
−0.300.....	<-6.00	4.042	7.093	2.232	5.037	−0.712	5.966
−0.400.....	<-6.00	4.039	7.128	2.374	5.126	−0.756	6.109
−0.500.....	<-6.00	4.035	7.161	2.519	5.211	−0.798	6.240
−0.600.....	<-6.00	4.031	7.193	2.672	5.292	−0.839	6.382
−0.700.....	<-6.00	4.027	7.229	2.840	5.377	−0.882	6.531
−0.800.....	<-6.00	4.025	7.270	3.040	5.469	−0.928	6.706
−0.900.....	<-6.00	4.037	7.349	3.407	5.618	−1.002	6.985
−0.993.....	−5.780	4.067	7.450	3.864	5.831	−1.109	7.304
−1.000.....	−5.670	4.071	7.461	3.911	5.852	−1.119	7.336
−1.100.....	−5.160	4.081	7.502	4.133	5.994	−1.190	7.496
−1.200.....	−4.878	4.082	7.517	4.266	6.096	−1.241	7.618
−1.300.....	−4.732	4.074	7.519	4.338	6.166	−1.276	7.687
−1.400.....	−4.576	4.069	7.521	4.429	6.245	−1.316	7.783
−1.500.....	−4.421	4.062	7.521	4.532	6.316	−1.351	7.870
−1.600.....	−4.340	4.052	7.509	4.589	6.376	−1.381	7.954
−1.700.....	−4.314	4.039	7.488	4.636	6.423	−1.405	8.036
−1.800.....	−4.328	4.024	7.461	4.678	6.464	−1.425	8.118
−1.900.....	−4.351	4.009	7.433	4.723	6.505	−1.446	8.202
−2.000.....	−4.374	3.994	7.404	4.762	6.544	−1.465	8.280
−2.100.....	−4.438	3.977	7.371	4.793	6.576	−1.481	8.356
−2.200.....	−4.540	3.959	7.337	4.823	6.607	−1.497	8.432
−2.300.....	−4.641	3.942	7.302	4.852	6.637	−1.511	8.507
−2.400.....	−4.769	3.923	7.265	4.875	6.662	−1.524	8.578
−2.500.....	−4.904	3.904	7.229	4.894	6.684	−1.535	8.644
−2.600.....	−5.053	3.884	7.192	4.911	6.705	−1.546	8.710
−2.700.....	−5.211	3.863	7.156	4.925	6.720	−1.553	8.772
−2.800.....	−5.386	3.842	7.118	4.938	6.736	−1.561	8.835
−2.900.....	−5.578	3.821	7.080	4.951	6.753	−1.570	8.899
−3.000.....	−5.792	3.800	7.039	4.962	6.768	−1.577	8.961
−3.100.....	−6.075	3.778	6.999	4.972	6.781	−1.584	9.023
−3.200.....	<-6.00	3.756	6.956	4.980	6.794	−1.590	9.086
−3.300.....	<-6.00	3.734	6.913	4.989	6.806	−1.596	9.149
−3.400.....	<-6.00	3.712	6.866	4.996	6.818	−1.602	9.214
−3.500.....	<-6.00	3.691	6.814	5.004	6.831	−1.609	9.284
−3.600.....	<-6.00	3.669	6.759	5.011	6.844	−1.615	9.354
−3.700.....	<-6.00	3.647	6.700	5.018	6.855	−1.621	9.422
−3.800.....	<-6.00	3.623	6.643	5.023	6.863	−1.625	9.483
−3.900.....	<-6.00	3.601	6.581	5.028	6.871	−1.629	9.546
−4.000.....	<-6.00	3.578	6.506	5.033	6.880	−1.633	9.618
−4.100.....	<-6.00	3.553	6.469	5.035	6.883	−1.635	9.652
−4.200.....	<-6.00	3.530	6.419	5.037	6.887	−1.637	9.700
−4.300.....	<-6.00	3.506	6.366	5.040	6.891	−1.639	9.750
−4.400.....	<-6.00	3.482	6.293	5.043	6.897	−1.642	9.817
−4.500.....	<-6.00	3.458	6.221	5.045	6.902	−1.644	9.879
−4.600.....	<-6.00	3.434	6.149	5.047	6.906	−1.646	9.936
−4.700.....	<-6.00	3.410	6.077	5.049	6.909	−1.648	9.991
−4.800.....	<-6.00	3.386	6.003	5.051	6.912	−1.649	10.046
−4.900.....	<-6.00	3.361	5.931	5.052	6.914	−1.650	10.096
−5.000.....	<-6.00	3.337	5.854	5.053	6.915	−1.651	10.147

peratures, which would eventually yield core helium ignition during the high photon luminosity phases (see § 4 for details).

In this study we employed the two theories of convection described in § 2. Particularly, in the framework of the MLT, we adopt the three popular versions associated with white dwarf work. Briefly, these are ML1, corresponding to the standard version of Böhm-Vitense (1958) with $\alpha = 1$; ML2, which has the same α as ML1, but a different choice of a, b, and c, which results in less horizontal energy loss and more efficient convection than ML1; and ML3, which is the same as ML2, but has $\alpha = 2$ (see Tassoul et al. 1990 for more details).

Tables 1–9 summarize the main features of our He WD

TABLE 3

SELECTED STAGES FOR A 0.20 $M_\odot$ HELIUM WHITE DWARF

log $L/L_\odot$	log $L_\nu/L_\odot$	log $T_{\rm eff}$	log T_c	log ρ_c	log g	log $R/R_\odot$	log (Age)
1.000	<-6.00	4.030	6.573	0.372	3.816	-0.039	$-\infty$
0.900	<-6.00	4.037	6.634	0.554	3.942	-0.102	4.497
0.800	<-6.00	4.039	6.687	0.714	4.052	-0.157	4.650
0.700	<-6.00	4.044	6.745	0.890	4.172	-0.217	4.815
0.600	<-6.00	4.046	6.797	1.048	4.280	-0.271	4.964
0.500	<-6.00	4.051	6.854	1.220	4.396	-0.329	5.123
0.400	<-6.00	4.054	6.909	1.389	4.511	-0.386	5.279
0.300	<-6.00	4.055	6.959	1.546	4.616	-0.439	5.424
0.200	<-6.00	4.058	7.008	1.718	4.726	-0.494	5.578
0.100	<-6.00	4.060	7.054	1.893	4.832	-0.547	5.730
0.000	<-6.00	4.060	7.097	2.067	4.934	-0.598	5.881
-0.100.....	<-6.00	4.062	7.144	2.274	5.043	-0.652	6.051
-0.200.....	<-6.00	4.065	7.200	2.515	5.153	-0.707	6.238
-0.272.....	<-6.00	4.095	7.376	3.222	5.345	-0.803	6.697
-0.252.....	-5.711	4.125	7.503	3.676	5.446	-0.854	6.926
-0.300.....	-5.030	4.150	7.576	3.955	5.593	-0.927	7.063
-0.369.....	-4.546	4.180	7.623	4.160	5.782	-1.022	7.170
-0.400.....	-4.393	4.188	7.636	4.226	5.845	-1.053	7.207
-0.500.....	-4.030	4.203	7.664	4.390	6.005	-1.133	7.308
-0.600.....	-3.776	4.208	7.677	4.509	6.125	-1.193	7.392
-0.700.....	-3.593	4.208	7.683	4.611	6.225	-1.243	7.470
-0.800.....	-3.445	4.205	7.684	4.696	6.312	-1.287	7.545
-0.900.....	-3.335	4.199	7.679	4.769	6.388	-1.325	7.616
-1.000.....	-3.256	4.189	7.666	4.827	6.451	-1.356	7.688
-1.100.....	-3.202	4.181	7.651	4.879	6.518	-1.390	7.759
-1.200.....	-3.182	4.173	7.632	4.926	6.584	-1.423	7.830
-1.300.....	-3.190	4.162	7.609	4.968	6.643	-1.452	7.901
-1.400.....	-3.223	4.150	7.582	5.006	6.694	-1.478	7.973
-1.500.....	-3.277	4.136	7.552	5.041	6.738	-1.500	8.044
-1.600.....	-3.352	4.121	7.519	5.072	6.776	-1.519	8.115
-1.700.....	-3.442	4.104	7.485	5.099	6.810	-1.536	8.184
-1.800.....	-3.544	4.087	7.451	5.122	6.840	-1.551	8.251
-1.900.....	-3.655	4.068	7.415	5.143	6.867	-1.564	8.317
-2.000.....	-3.787	4.049	7.379	5.162	6.891	-1.576	8.383
-2.100.....	-3.939	4.030	7.342	5.178	6.912	-1.587	8.450
-2.200.....	-4.102	4.009	7.305	5.193	6.931	-1.596	8.515
-2.300.....	-4.278	3.989	7.268	5.206	6.949	-1.605	8.579
-2.400.....	-4.467	3.968	7.230	5.217	6.964	-1.613	8.643
-2.500.....	-4.669	3.946	7.193	5.227	6.977	-1.619	8.704
-2.600.....	-4.885	3.924	7.154	5.236	6.989	-1.625	8.765
-2.700.....	-5.123	3.902	7.115	5.245	7.001	-1.631	8.828
-2.800.....	-5.381	3.880	7.075	5.252	7.012	-1.637	8.890
-2.900.....	-5.666	3.857	7.035	5.259	7.023	-1.642	8.952
-3.000.....	<-6.00	3.835	6.993	5.265	7.032	-1.647	9.015
-3.100.....	<-6.00	3.812	6.950	5.271	7.041	-1.651	9.078
-3.200.....	<-6.00	3.789	6.907	5.276	7.049	-1.655	9.141
-3.300.....	<-6.00	3.766	6.862	5.281	7.057	-1.659	9.204
-3.400.....	<-6.00	3.743	6.816	5.285	7.064	-1.663	9.268
-3.500.....	<-6.00	3.719	6.769	5.289	7.071	-1.666	9.331
-3.600.....	<-6.00	3.696	6.711	5.294	7.080	-1.670	9.405
-3.700.....	<-6.00	3.673	6.649	5.298	7.087	-1.674	9.477
-3.800.....	<-6.00	3.650	6.586	5.301	7.094	-1.678	9.545
-3.900.....	<-6.00	3.626	6.520	5.304	7.099	-1.680	9.611
-4.000.....	<-6.00	3.602	6.468	5.306	7.103	-1.682	9.663
-4.100.....	<-6.00	3.578	6.416	5.308	7.107	-1.684	9.713
-4.200.....	<-6.00	3.554	6.366	5.310	7.109	-1.685	9.763
-4.300.....	<-6.00	3.530	6.315	5.311	7.112	-1.687	9.813
-4.400.....	<-6.00	3.505	6.261	5.313	7.114	-1.688	9.867
-4.500.....	<-6.00	3.481	6.187	5.314	7.118	-1.690	9.937
-4.600.....	<-6.00	3.457	6.115	5.315	7.121	-1.691	10.000
-4.700.....	<-6.00	3.432	6.045	5.317	7.123	-1.692	10.059
-4.800.....	<-6.00	3.408	5.973	5.318	7.125	-1.693	10.116
-4.900.....	<-6.00	3.383	5.900	5.318	7.126	-1.694	10.171
-5.000.....	<-6.00	3.358	5.826	5.319	7.127	-1.694	10.225

evolutionary models according to the CMT. For each table and from left to right we list the photon and neutrino luminosities (both in solar units), the effective ($T_{\rm eff}$) and central (T_c) temperatures, the central density ρ_c, the surface gravity g, the stellar radius R (in solar units), and the age (in years). Since we are not computing any of the binary evolution that leads to the formation of these helium objects, we elect to count the age from the first model considered here. We want to mention that, at low luminosities, the quantities listed in the tables are practically insensitive to the theories of convection we employed because the temperature stratification becomes basically adiabatic in most of the OCZ by the time

TABLE 4

SELECTED STAGES FOR A 0.25 $M_\odot$ HELIUM WHITE DWARF

log $L/L_\odot$	log $L_w/L_\odot$	log $T_{\rm eff}$	log T_c	log ρ_c	log g	log $R/R_\odot$	log (Age)
1.000	< -6.00	4.041	6.686	0.520	3.953	−0.059	$-\infty$
0.900	< -6.00	4.045	6.743	0.694	4.072	−0.118	4.650
0.800	< -6.00	4.049	6.800	0.866	4.188	−0.176	4.821
0.700	< -6.00	4.053	6.856	1.034	4.302	−0.233	4.984
0.600	< -6.00	4.056	6.908	1.205	4.415	−0.290	5.143
0.500	< -6.00	4.059	6.957	1.383	4.527	−0.346	5.300
0.400	< -6.00	4.064	7.008	1.584	4.645	−0.405	5.467
0.300	< -6.00	4.066	7.058	1.792	4.755	−0.460	5.637
0.200	< -6.00	4.070	7.117	2.040	4.872	−0.518	5.835
0.182	< -6.00	4.100	7.352	2.928	5.011	−0.588	6.380
0.217	< -6.00	4.130	7.454	3.262	5.096	−0.630	6.523
0.227	−5.740	4.160	7.521	3.482	5.206	−0.685	6.612
0.225	−5.372	4.190	7.565	3.630	5.328	−0.746	6.665
0.217	−4.996	4.220	7.609	3.784	5.456	−0.810	6.720
0.200	−4.606	4.250	7.653	3.945	5.592	−0.878	6.780
0.169	−4.193	4.280	7.698	4.118	5.744	−0.954	6.848
0.110	−3.734	4.310	7.745	4.317	5.923	−1.044	6.933
0.100	−3.644	4.317	7.754	4.355	5.957	−1.061	6.950
0.000	−3.203	4.339	7.793	4.555	6.147	−1.156	7.050
−0.100.....	−2.921	4.347	7.811	4.688	6.279	−1.222	7.130
−0.200.....	−2.687	4.350	7.822	4.799	6.391	−1.278	7.205
−0.300.....	−2.566	4.346	7.823	4.887	6.476	−1.320	7.272
−0.400.....	−2.452	4.340	7.821	4.960	6.550	−1.357	7.343
−0.500.....	−2.391	4.330	7.810	5.014	6.609	−1.387	7.413
−0.600.....	−2.322	4.318	7.794	5.062	6.663	−1.414	7.484
−0.700.....	−2.280	4.306	7.777	5.111	6.715	−1.440	7.555
−0.800.....	−2.266	4.293	7.757	5.154	6.763	−1.464	7.625
−0.900.....	−2.274	4.279	7.734	5.194	6.806	−1.485	7.695
−1.000.....	−2.301	4.264	7.708	5.230	6.846	−1.505	7.764
−1.100.....	−2.358	4.248	7.678	5.261	6.881	−1.523	7.835
−1.200.....	−2.442	4.231	7.644	5.290	6.914	−1.539	7.907
−1.300.....	−2.534	4.213	7.610	5.316	6.944	−1.554	7.976
−1.400.....	−2.647	4.198	7.574	5.338	6.983	−1.574	8.044
−1.500.....	−2.772	4.181	7.537	5.359	7.015	−1.590	8.112
−1.600.....	−2.908	4.163	7.501	5.377	7.044	−1.604	8.177
−1.700.....	−3.052	4.145	7.464	5.393	7.070	−1.617	8.241
−1.800.....	−3.206	4.125	7.427	5.407	7.091	−1.628	8.304
−1.900.....	−3.364	4.105	7.390	5.419	7.110	−1.638	8.368
−2.000.....	−3.561	4.084	7.351	5.431	7.127	−1.646	8.433
−2.100.....	−3.762	4.063	7.314	5.441	7.142	−1.654	8.496
−2.200.....	−3.975	4.041	7.276	5.450	7.156	−1.660	8.559
−2.300.....	−4.203	4.019	7.237	5.458	7.168	−1.666	8.622
−2.400.....	−4.447	3.997	7.199	5.465	7.179	−1.672	8.683
−2.500.....	−4.703	3.974	7.160	5.472	7.188	−1.676	8.744
−2.600.....	−4.984	3.952	7.121	5.478	7.197	−1.681	8.807
−2.700.....	−5.283	3.929	7.081	5.483	7.206	−1.685	8.870
−2.800.....	−5.602	3.906	7.040	5.488	7.214	−1.689	8.933
−2.900.....	−5.971	3.883	6.998	5.493	7.221	−1.693	8.996
−3.000.....	< -6.00	3.859	6.956	5.497	7.228	−1.696	9.060
−3.100.....	< -6.00	3.836	6.912	5.501	7.235	−1.700	9.124
−3.200.....	< -6.00	3.813	6.867	5.504	7.241	−1.703	9.188
−3.300.....	< -6.00	3.789	6.821	5.508	7.246	−1.705	9.252
−3.400.....	< -6.00	3.765	6.774	5.511	7.251	−1.708	9.317
−3.500.....	< -6.00	3.741	6.726	5.513	7.256	−1.710	9.381
−3.600.....	< -6.00	3.718	6.676	5.516	7.261	−1.713	9.446
−3.700.....	< -6.00	3.694	6.611	5.519	7.267	−1.716	9.524
−3.800.....	< -6.00	3.670	6.545	5.521	7.272	−1.718	9.597
−3.900.....	< -6.00	3.646	6.472	5.523	7.277	−1.721	9.672
−4.000.....	< -6.00	3.622	6.427	5.525	7.279	−1.722	9.716
−4.100.....	< -6.00	3.598	6.375	5.526	7.281	−1.723	9.768
−4.200.....	< -6.00	3.573	6.324	5.527	7.283	−1.724	9.820
−4.300.....	< -6.00	3.549	6.273	5.528	7.285	−1.725	9.871
−4.400.....	< -6.00	3.524	6.222	5.529	7.287	−1.726	9.923
−4.500.....	< -6.00	3.499	6.167	5.530	7.288	−1.726	9.979
−4.600.....	< -6.00	3.475	6.090	5.531	7.291	−1.728	10.053
−4.700.....	< -6.00	3.450	6.017	5.532	7.292	−1.728	10.118
−4.800.....	< -6.00	3.426	5.947	5.532	7.294	−1.729	10.175
−4.900.....	< -6.00	3.401	5.876	5.533	7.295	−1.730	10.232
−5.000.....	< -6.00	3.376	5.803	5.534	7.296	−1.730	10.287

TABLE 5

SELECTED STAGES FOR A 0.30 $M_\odot$ HELIUM WHITE DWARF

log $L/L_\odot$	log $L_w/L_\odot$	log $T_{\rm eff}$	log T_c	log ρ_c	log g	log $R/R_\odot$	log (Age)
1.000	< -6.00	4.046	6.774	0.630	4.055	−0.070	$-\infty$
0.900	< -6.00	4.052	6.833	0.814	4.179	−0.132	4.813
0.800	< -6.00	4.057	6.885	1.000	4.297	−0.191	4.983
0.700	< -6.00	4.061	6.935	1.193	4.413	−0.249	5.157
0.600	< -6.00	4.064	6.985	1.398	4.525	−0.305	5.321
0.500	< -6.00	4.068	7.043	1.642	4.642	−0.364	5.503
0.400	< -6.00	4.075	7.130	1.998	4.771	−0.428	5.746
0.547	< -6.00	4.105	7.384	2.862	4.743	−0.414	6.175
0.559	< -6.00	4.135	7.429	3.000	4.851	−0.468	6.232
0.570	< -6.00	4.165	7.473	3.139	4.961	−0.523	6.282
0.578	−5.837	4.195	7.517	3.279	5.073	−0.579	6.331
0.584	−5.480	4.225	7.561	3.423	5.187	−0.636	6.380
0.587	−5.120	4.255	7.606	3.569	5.303	−0.694	6.429
0.587	−4.754	4.285	7.651	3.719	5.423	−0.754	6.480
0.582	−4.381	4.315	7.695	3.872	5.549	−0.817	6.533
0.569	−4.000	4.345	7.740	4.032	5.681	−0.883	6.590
0.546	−3.605	4.375	7.786	4.202	5.825	−0.955	6.652
0.503	−3.183	4.405	7.832	4.389	5.988	−1.036	6.727
0.417	−2.692	4.435	7.880	4.615	6.194	−1.140	6.829
0.300	−2.264	4.455	7.915	4.823	6.391	−1.238	6.937
0.200	−1.980	4.462	7.932	4.954	6.519	−1.302	7.016
0.100	−1.820	4.461	7.937	5.048	6.615	−1.350	7.084
0.000	−1.721	4.455	7.935	5.128	6.690	−1.388	7.149
−0.100.....	−1.654	4.445	7.926	5.182	6.751	−1.418	7.216
−0.200.....	−1.611	4.432	7.911	5.226	6.800	−1.443	7.282
−0.300.....	−1.555	4.419	7.894	5.269	6.847	−1.466	7.350
−0.400.....	−1.523	4.407	7.875	5.315	6.896	−1.491	7.418
−0.500.....	−1.519	4.393	7.853	5.356	6.940	−1.513	7.486
−0.600.....	−1.534	4.378	7.828	5.393	6.980	−1.533	7.552
−0.700.....	−1.578	4.361	7.799	5.425	7.015	−1.550	7.617
−0.800.....	−1.639	4.345	7.768	5.455	7.048	−1.567	7.682
−0.900.....	−1.717	4.327	7.735	5.482	7.079	−1.582	7.748
−1.000.....	−1.818	4.309	7.700	5.506	7.106	−1.596	7.815
−1.100.....	−1.930	4.291	7.664	5.528	7.133	−1.609	7.882
−1.200.....	−2.060	4.271	7.628	5.547	7.156	−1.621	7.947
−1.300.....	−2.197	4.252	7.591	5.564	7.178	−1.632	8.012
−1.400.....	−2.354	4.232	7.554	5.580	7.197	−1.641	8.077
−1.500.....	−2.520	4.212	7.516	5.593	7.217	−1.651	8.142
−1.600.....	−2.693	4.193	7.479	5.605	7.243	−1.664	8.205
−1.700.....	−2.875	4.173	7.442	5.616	7.264	−1.675	8.268
−1.800.....	−3.069	4.153	7.404	5.625	7.280	−1.683	8.332
−1.900.....	−3.281	4.131	7.365	5.634	7.295	−1.690	8.398
−2.000.....	−3.512	4.110	7.326	5.642	7.309	−1.697	8.462
−2.100.....	−3.758	4.088	7.288	5.649	7.320	−1.703	8.526
−2.200.....	−4.018	4.065	7.249	5.655	7.330	−1.708	8.589
−2.300.....	−4.293	4.042	7.210	5.661	7.339	−1.712	8.653
−2.400.....	−4.580	4.019	7.171	5.666	7.347	−1.716	8.715
−2.500.....	−4.889	3.996	7.132	5.671	7.355	−1.720	8.779
−2.600.....	−5.212	3.973	7.092	5.675	7.362	−1.724	8.842
−2.700.....	−5.553	3.950	7.051	5.679	7.369	−1.727	8.906
−2.800.....	−5.919	3.926	7.010	5.683	7.375	−1.730	8.970
−2.900.....	< -6.00	3.903	6.967	5.686	7.380	−1.733	9.035
−3.000.....	< -6.00	3.879	6.924	5.689	7.386	−1.736	9.099
−3.100.....	< -6.00	3.855	6.880	5.692	7.391	−1.738	9.164
−3.200.....	< -6.00	3.831	6.834	5.695	7.395	−1.740	9.230
−3.300.....	< -6.00	3.807	6.787	5.697	7.400	−1.743	9.295
−3.400.....	< -6.00	3.783	6.739	5.699	7.404	−1.744	9.360
−3.500.....	< -6.00	3.759	6.690	5.701	7.407	−1.746	9.425
−3.600.....	< -6.00	3.735	6.638	5.703	7.411	−1.748	9.492
−3.700.....	< -6.00	3.711	6.583	5.705	7.414	−1.750	9.559
−3.800.....	< -6.00	3.687	6.515	5.707	7.419	−1.752	9.638
−3.900.....	< -6.00	3.663	6.447	5.709	7.422	−1.754	9.710
−4.000.....	< -6.00	3.639	6.393	5.710	7.424	−1.755	9.765
−4.100.....	< -6.00	3.614	6.341	5.711	7.426	−1.756	9.817
−4.200.....	< -6.00	3.589	6.289	5.712	7.428	−1.757	9.870
−4.300.....	< -6.00	3.565	6.238	5.712	7.429	−1.757	9.922
−4.400.....	< -6.00	3.540	6.188	5.713	7.430	−1.758	9.973
−4.500.....	< -6.00	3.515	6.137	5.714	7.431	−1.758	10.027
−4.600.....	< -6.00	3.491	6.072	5.714	7.433	−1.759	10.093
−4.700.....	< -6.00	3.466	5.997	5.715	7.434	−1.760	10.162
−4.800.....	< -6.00	3.441	5.925	5.716	7.435	−1.760	10.225
−4.900.....	< -6.00	3.417	5.855	5.716	7.436	−1.761	10.283
−5.000.....	< -6.00	3.392	5.782	5.717	7.437	−1.761	10.339

TABLE 6

SELECTED STAGES FOR A 0.35 $M_\odot$ HELIUM WHITE DWARF

log $L/L_\odot$	log $L_\nu/L_\odot$	log $T_{\rm eff}$	log T_c	log ρ_c	log g	log $R/R_\odot$	log (Age)
−0.500.....	−1.012	4.435	7.848	5.615	7.178	−1.598	−∞
−0.600.....	−1.088	4.418	7.815	5.641	7.208	−1.613	7.555
−0.700.....	−1.180	4.399	7.782	5.665	7.234	−1.626	7.617
−0.800.....	−1.287	4.381	7.748	5.686	7.259	−1.639	7.679
−0.900.....	−1.408	4.361	7.714	5.705	7.282	−1.650	7.741
−1.000.....	−1.543	4.342	7.679	5.722	7.304	−1.661	7.805
−1.100.....	−1.689	4.322	7.644	5.737	7.323	−1.671	7.869
−1.200.....	−1.848	4.301	7.609	5.751	7.341	−1.680	7.933
−1.300.....	−2.021	4.280	7.572	5.763	7.357	−1.688	7.999
−1.400.....	−2.207	4.259	7.535	5.774	7.373	−1.695	8.065
−1.500.....	−2.403	4.237	7.497	5.784	7.387	−1.702	8.132
−1.600.....	−2.609	4.217	7.459	5.793	7.404	−1.711	8.198
−1.700.....	−2.825	4.196	7.421	5.801	7.420	−1.719	8.265
−1.800.....	−3.052	4.174	7.382	5.808	7.434	−1.726	8.333
−1.900.....	−3.310	4.152	7.342	5.815	7.447	−1.732	8.401
−2.000.....	−3.581	4.130	7.303	5.821	7.457	−1.738	8.468
−2.100.....	−3.865	4.107	7.264	5.826	7.467	−1.743	8.534
−2.200.....	−4.164	4.084	7.225	5.831	7.475	−1.747	8.599
−2.300.....	−4.473	4.061	7.186	5.835	7.482	−1.750	8.664
−2.400.....	−4.798	4.038	7.147	5.839	7.489	−1.753	8.729
−2.500.....	−5.138	4.014	7.107	5.843	7.495	−1.757	8.794
−2.600.....	−5.492	3.991	7.066	5.847	7.500	−1.759	8.859
−2.700.....	−5.890	3.967	7.025	5.850	7.506	−1.762	8.924
−2.800.....	< −6.00	3.943	6.983	5.852	7.511	−1.765	8.989
−2.900.....	< −6.00	3.920	6.940	5.855	7.515	−1.767	9.055
−3.000.....	< −6.00	3.896	6.896	5.858	7.520	−1.769	9.121
−3.100.....	< −6.00	3.872	6.851	5.860	7.524	−1.771	9.187
−3.200.....	< −6.00	3.848	6.804	5.862	7.527	−1.773	9.254
−3.300.....	< −6.00	3.823	6.757	5.864	7.531	−1.775	9.320
−3.400.....	< −6.00	3.799	6.708	5.865	7.534	−1.776	9.387
−3.500.....	< −6.00	3.775	6.657	5.867	7.537	−1.778	9.454
−3.600.....	< −6.00	3.751	6.606	5.869	7.540	−1.779	9.520
−3.700.....	< −6.00	3.726	6.553	5.870	7.542	−1.780	9.586
−3.800.....	< −6.00	3.702	6.490	5.871	7.545	−1.782	9.660
−3.900.....	< −6.00	3.678	6.427	5.873	7.548	−1.783	9.729
−4.000.....	< −6.00	3.653	6.369	5.874	7.550	−1.784	9.791
−4.100.....	< −6.00	3.629	6.314	5.874	7.551	−1.785	9.848
−4.200.....	< −6.00	3.604	6.261	5.875	7.553	−1.786	9.902
−4.300.....	< −6.00	3.579	6.209	5.876	7.554	−1.786	9.955
−4.400.....	< −6.00	3.554	6.159	5.876	7.555	−1.787	10.007
−4.500.....	< −6.00	3.530	6.108	5.877	7.556	−1.787	10.060
−4.600.....	< −6.00	3.505	6.051	5.877	7.557	−1.787	10.119
−4.700.....	< −6.00	3.480	5.979	5.878	7.558	−1.788	10.189
−4.800.....	< −6.00	3.455	5.908	5.878	7.559	−1.789	10.254
−4.900.....	< −6.00	3.431	5.837	5.879	7.559	−1.789	10.314
−5.000.....	< −6.00	3.406	5.766	5.879	7.560	−1.789	10.370

its base penetrates into the degenerate core at low $T_{\rm eff}$ (see Fontaine & Van Horn 1976 and Tassoul et al. 1990). Accordingly, the cooling properties of the models at low luminosities do not depend upon a detailed knowledge of the convection theory. As mentioned in § 4, for models with $M > 0.30\ M_\odot$, the first tabulated row corresponds to the case in which the nuclear energy content of the whole model due to helium burning can be assumed to be negligible [$\log (L_{\rm nuclear}/L_\odot) \lesssim -3$], which would not be the situation for slightly higher $T_{\rm eff}$. In Table 10, we list the radius (in solar units) and the central density as given by the models of H-S for pure helium configurations of a given mass at zero temperature.

In Figure 1 we show the evolution of our models in the HR diagram according to the CMT together with the lowest part of the hydrogen-rich ZAMS calculated by D'Antona and Mazzitelli (1994) for stars from 0.08 to ≈ 2 $M_\odot$. In this figure, only for the sake of reference, we have also included the *approximate* location of the low-mass, helium ZAMS calculated for stars up to 0.29 $M_\odot$ assuming that the temporal derivative of the entropy is negligible. As discussed in § 4, there is no conflict between the location of the helium ZAMS and our 0.3 $M_\odot$ evolutionary model results because the ZAMS models do not include the temporal derivative of the entropy. As expected in the WD regime, more massive models at a fixed $T_{\rm eff}$ have lower luminosities owing to their smaller radii (Chandrasekhar 1939). In this regime, the WD radius gradually becomes smaller as the luminosity decreases, eventually reaching an almost constant value as expected for a configuration subject to strong degeneracy, in which the mechanical and thermal properties are almost decoupled from each other. This behavior can be better understood in terms of the evolution of the central region of models shown in Figure 2. In fact, at sufficiently low luminosities, the mechanical structure of the model is specified primarily by degenerate electron pressure, because finite-temperature effects are negligible. As a result, the central density asymptotically reaches a constant value corresponding to a zero temperature configuration. In the HR diagram, this situation is

TABLE 7

SELECTED STAGES FOR A 0.40 $M_\odot$ HELIUM WHITE DWARF

log $L/L_\odot$	log $L_\nu/L_\odot$	log $T_{\rm eff}$	log T_c	log ρ_c	log g	log $R/R_\odot$	log (Age)
−0.500.....	−0.719	4.467	7.814	5.824	7.365	−1.662	−∞
−0.600.....	−0.827	4.448	7.784	5.843	7.387	−1.674	7.541
−0.700.....	−0.946	4.428	7.755	5.860	7.408	−1.684	7.597
−0.800.....	−1.077	4.408	7.724	5.875	7.427	−1.694	7.656
−0.900.....	−1.220	4.388	7.693	5.889	7.445	−1.703	7.717
−1.000.....	−1.376	4.367	7.661	5.901	7.462	−1.711	7.780
−1.100.....	−1.545	4.346	7.628	5.912	7.477	−1.719	7.846
−1.200.....	−1.730	4.324	7.592	5.923	7.491	−1.726	7.914
−1.300.....	−1.931	4.302	7.556	5.932	7.505	−1.733	7.984
−1.400.....	−2.145	4.280	7.518	5.941	7.517	−1.739	8.056
−1.500.....	−2.370	4.258	7.480	5.949	7.528	−1.744	8.128
−1.600.....	−2.606	4.236	7.441	5.956	7.540	−1.750	8.200
−1.700.....	−2.848	4.215	7.402	5.962	7.553	−1.757	8.273
−1.800.....	−3.122	4.193	7.362	5.968	7.565	−1.763	8.346
−1.900.....	−3.412	4.170	7.322	5.973	7.575	−1.768	8.417
−2.000.....	−3.715	4.147	7.283	5.978	7.584	−1.772	8.487
−2.100.....	−4.030	4.124	7.244	5.982	7.592	−1.776	8.556
−2.200.....	−4.354	4.101	7.205	5.986	7.599	−1.780	8.624
−2.300.....	−4.689	4.077	7.165	5.989	7.605	−1.782	8.691
−2.400.....	−5.037	4.054	7.126	5.993	7.610	−1.785	8.758
−2.500.....	−5.398	4.030	7.085	5.996	7.615	−1.788	8.825
−2.600.....	−5.774	4.006	7.044	5.998	7.620	−1.790	8.892
−2.700.....	< −6.00	3.982	7.003	6.001	7.625	−1.792	8.958
−2.800.....	< −6.00	3.958	6.960	6.003	7.629	−1.795	9.026
−2.900.....	< −6.00	3.934	6.916	6.005	7.632	−1.796	9.093
−3.000.....	< −6.00	3.910	6.872	6.007	7.636	−1.798	9.160
−3.100.....	< −6.00	3.886	6.826	6.009	7.639	−1.800	9.227
−3.200.....	< −6.00	3.862	6.779	6.011	7.642	−1.801	9.295
−3.300.....	< −6.00	3.838	6.731	6.013	7.645	−1.803	9.363
−3.400.....	< −6.00	3.813	6.681	6.014	7.648	−1.804	9.430
−3.500.....	< −6.00	3.789	6.630	6.015	7.650	−1.805	9.497
−3.600.....	< −6.00	3.764	6.578	6.016	7.652	−1.806	9.563
−3.700.....	< −6.00	3.740	6.525	6.018	7.654	−1.807	9.629
−3.800.....	< −6.00	3.715	6.470	6.019	7.656	−1.808	9.695
−3.900.....	< −6.00	3.691	6.408	6.020	7.659	−1.810	9.766
−4.000.....	< −6.00	3.666	6.347	6.020	7.660	−1.810	9.832
−4.100.....	< −6.00	3.642	6.290	6.021	7.662	−1.811	9.891
−4.200.....	< −6.00	3.617	6.236	6.022	7.663	−1.812	9.947
−4.300.....	< −6.00	3.592	6.184	6.022	7.664	−1.812	10.001
−4.400.....	< −6.00	3.567	6.133	6.023	7.665	−1.813	10.053
−4.500.....	< −6.00	3.543	6.083	6.023	7.665	−1.813	10.106
−4.600.....	< −6.00	3.518	6.031	6.023	7.666	−1.813	10.160
−4.700.....	< −6.00	3.493	5.966	6.024	7.667	−1.814	10.226
−4.800.....	< −6.00	3.468	5.893	6.024	7.668	−1.814	10.293
−4.900.....	< −6.00	3.443	5.822	6.025	7.668	−1.814	10.354
−5.000.....	< −6.00	3.418	5.752	6.025	7.669	−1.815	10.411

translated as evolutionary tracks following lines of constant radius. At intermediate luminosities, the effects of finite temperature on the EOS are apparent, particularly for less massive models (see Fig. 2). In this regime, the evolutionary tracks are insensitive to the treatment of convection. By contrast, in the high-luminosity range, low-mass models are fully convective, and their evolutionary paths depend quite strongly on the efficiency of convection. This can be appreciated clearly in Figures 3, 4, 5, 6, and 7. Each of these figures shows, for a given stellar mass, the evolution in the HR diagram according to the three versions of the MLT and the CMT.

Let us interpret this behavior. Low-mass objects have lower internal densities and thus higher opacities, which favor the occurrence of convection. The lower the stellar mass, the higher the fraction of the total mass in convective equilibrium. As cooling proceeds, the central region of the models gets closer to the conditions at which conduction inhibits convection. This causes the base of the OCZ to retreat toward the surface. From there on, differences in stellar radii resulting from different convective efficiencies will be less noticeable. In fact, such differences will be at most, comparable to the thickness of the OCZ. In the HR diagram, the tracks are sensitive to the total radius; so, as the OCZ gets thinner, the *fractional* difference in the radii of the models becomes smaller, making the tracks converge. This will occur sooner the thinner the OCZ is (i.e., the higher the stellar mass is).

The most important physics feature affecting the evolution of hot He WDs is neutrino emission. The behavior of neutrino luminosity L_ν is displayed in Figure 8 as a function of the (photon) luminosity L (the various neutrino emission processes are taken simultaneously). Neutrino cooling is important only during the high $T_{\rm eff}$ phases principally for the more massive models. Omitting neutrino cooling would result in models with considerably larger central temperatures, higher thermal pressures, and larger radii. As $T_{\rm eff}$ decreases, the neutrino luminosity fades away faster than the photon luminosity and neutrino cooling has little effect on the subsequent evolution of the models. Neutrino losses

TABLE 8

SELECTED STAGES FOR A 0.45 $M_\odot$ HELIUM WHITE DWARF

log $L/L_\odot$	log $L_\nu/L_\odot$	log $T_{\rm eff}$	log T_c	log ρ_c	log g	log $R/R_\odot$	log (Age)
−0.300.....	−0.325	4.533	7.829	5.971	7.478	−1.694	−∞
−0.400.....	−0.432	4.513	7.804	5.987	7.499	−1.704	7.388
−0.500.....	−0.545	4.493	7.780	6.002	7.519	−1.714	7.439
−0.600.....	−0.667	4.473	7.756	6.015	7.536	−1.723	7.493
−0.700.....	−0.799	4.452	7.732	6.027	7.553	−1.731	7.549
−0.800.....	−0.943	4.431	7.706	6.039	7.568	−1.739	7.608
−0.900.....	−1.101	4.409	7.677	6.049	7.583	−1.746	7.671
−1.000.....	−1.274	4.388	7.647	6.059	7.596	−1.753	7.737
−1.100.....	−1.464	4.366	7.614	6.068	7.609	−1.759	7.807
−1.200.....	−1.674	4.344	7.579	6.076	7.621	−1.765	7.882
−1.300.....	−1.903	4.321	7.541	6.084	7.632	−1.770	7.961
−1.400.....	−2.145	4.299	7.502	6.091	7.642	−1.775	8.040
−1.500.....	−2.398	4.276	7.463	6.097	7.651	−1.780	8.119
−1.600.....	−2.663	4.253	7.424	6.103	7.660	−1.784	8.199
−1.700.....	−2.938	4.231	7.383	6.108	7.671	−1.790	8.278
−1.800.....	−3.246	4.209	7.344	6.113	7.681	−1.795	8.355
−1.900.....	−3.562	4.186	7.304	6.117	7.689	−1.799	8.430
−2.000.....	−3.889	4.163	7.265	6.121	7.697	−1.803	8.503
−2.100.....	−4.225	4.139	7.225	6.125	7.703	−1.806	8.574
−2.200.....	−4.566	4.116	7.186	6.128	7.709	−1.809	8.644
−2.300.....	−4.919	4.092	7.147	6.131	7.714	−1.812	8.713
−2.400.....	−5.282	4.068	7.106	6.134	7.719	−1.814	8.782
−2.500.....	−5.656	4.044	7.066	6.136	7.723	−1.816	8.850
−2.600.....	< −6.00	4.020	7.024	6.138	7.727	−1.818	8.918
−2.700.....	< −6.00	3.996	6.982	6.141	7.731	−1.820	8.986
−2.800.....	< −6.00	3.972	6.939	6.143	7.735	−1.822	9.054
−2.900.....	< −6.00	3.948	6.895	6.144	7.738	−1.824	9.123
−3.000.....	< −6.00	3.924	6.850	6.146	7.741	−1.825	9.191
−3.100.....	< −6.00	3.899	6.804	6.148	7.744	−1.826	9.259
−3.200.....	< −6.00	3.875	6.756	6.149	7.746	−1.828	9.328
−3.300.....	< −6.00	3.851	6.707	6.150	7.749	−1.829	9.397
−3.400.....	< −6.00	3.826	6.656	6.152	7.751	−1.830	9.465
−3.500.....	< −6.00	3.802	6.605	6.153	7.753	−1.831	9.533
−3.600.....	< −6.00	3.777	6.553	6.154	7.755	−1.832	9.599
−3.700.....	< −6.00	3.753	6.500	6.155	7.756	−1.833	9.664
−3.800.....	< −6.00	3.728	6.450	6.155	7.758	−1.834	9.724
−3.900.....	< −6.00	3.703	6.391	6.156	7.760	−1.834	9.794
−4.000.....	< −6.00	3.679	6.329	6.157	7.761	−1.835	9.864
−4.100.....	< −6.00	3.654	6.271	6.158	7.762	−1.836	9.925
−4.200.....	< −6.00	3.629	6.215	6.158	7.763	−1.836	9.983
−4.300.....	< −6.00	3.605	6.162	6.159	7.764	−1.837	10.038
−4.400.....	< −6.00	3.580	6.111	6.159	7.765	−1.837	10.090
−4.500.....	< −6.00	3.555	6.061	6.159	7.765	−1.837	10.142
−4.600.....	< −6.00	3.530	6.010	6.160	7.766	−1.838	10.195
−4.700.....	< −6.00	3.505	5.953	6.160	7.766	−1.838	10.253
−4.800.....	< −6.00	3.480	5.881	6.160	7.767	−1.838	10.321
−4.900.....	< −6.00	3.455	5.810	6.161	7.768	−1.838	10.384
−5.000.....	< −6.00	3.431	5.739	6.161	7.768	−1.839	10.441

cause the maximum temperature $T_{\rm max}$ to occur away from the center of the model. This is shown in Figure 9, where we plot the location of $T_{\rm max}$ in the Lagrangian coordinate as a function of photon luminosity for 0.4, 0.45, and 0.5 $M_\odot$ He WD models. For lower stellar masses or lower luminosities, $T_{\rm max}$ occurs in the center throughout the entire evolution. Note that for the three models, $T_{\rm max}$ reaches the center at approximately the same luminosity. For the same models, the central and maximum temperatures versus central density are shown in Figure 10. During the phase of strong neutrino losses, $T_{\rm max}$ differs appreciably from the central temperature. From the analysis of Figures 8–10, it is clear that neutrino losses considerably affects both the cooling and structural properties of the more massive He WD configurations, and therefore they must be taken into account in detailed evolutionary studies of these objects.

In order to further clarify this point, we show in Figure 11 the fractional luminosity vs. the mass fraction for the 0.45 $M_\odot$ model at log $T_{\rm eff} = 4.54$, 4.42, and 4.34. As a result of neutrino emission, the luminosity $L(r)$ is not proportional to the mass $M(r)$ in the hot-WD interior. However, as the WD cools down, it comes closer to satisfying the proportionality relation. By $T_{\rm eff} = 20{,}000$ K, neutrino cooling effects are small enough to make $L(r) \propto M(r)$ satisfactory.

The change of the radius R and surface gravity g of our models with cooling according to the CMT is shown in Figures 12 and 13, respectively. Only the values corresponding to the WD regime are depicted. Except for the least massive models in the high $T_{\rm eff}$ domain, the values shown in the figures are insensitive to the different theories of convection employed in this study. The main observation we can make from these figures is the substantial deviation of radii and surface gravities of our hot, low-mass models from those given by H-S zero temperature configurations for pure-helium compositions. For instance, at $T_{\rm eff} \approx 25{,}000$ K, the radius of the 0.3 $M_\odot$ model is twice the H-S radius and even at 15,000 K the difference is 25%. Because finite-temperature effects are proportionally greater in less

TABLE 9

SELECTED STAGES FOR A 0.5 $M_\odot$ HELIUM WHITE DWARF

log $L/L_\odot$	log $L_\nu/L_\odot$	log $T_{\rm eff}$	log T_c	log ρ_c	log g	log $R/R_\odot$	log (Age)
−0.300	−0.196	4.557	7.795	6.136	7.618	−1.741	−∞
−0.400	−0.310	4.536	7.776	6.148	7.635	−1.749	7.326
−0.500	−0.430	4.515	7.757	6.158	7.651	−1.757	7.377
−0.600	−0.559	4.493	7.738	6.168	7.665	−1.764	7.431
−0.700	−0.699	4.472	7.717	6.178	7.679	−1.771	7.489
−0.800	−0.854	4.450	7.693	6.186	7.691	−1.777	7.551
−0.900	−1.025	4.428	7.667	6.195	7.703	−1.783	7.619
−1.000	−1.215	4.406	7.637	6.202	7.714	−1.789	7.692
−1.100	−1.429	4.383	7.604	6.210	7.725	−1.794	7.771
−1.200	−1.668	4.361	7.566	6.217	7.735	−1.799	7.856
−1.300	−1.925	4.338	7.527	6.224	7.745	−1.804	7.944
−1.400	−2.195	4.315	7.487	6.230	7.753	−1.808	8.032
−1.500	−2.475	4.292	7.448	6.235	7.761	−1.812	8.119
−1.600	−2.759	4.269	7.407	6.240	7.768	−1.816	8.206
−1.700	−3.074	4.246	7.367	6.245	7.777	−1.820	8.289
−1.800	−3.403	4.223	7.327	6.249	7.785	−1.824	8.369
−1.900	−3.739	4.200	7.287	6.252	7.793	−1.828	8.446
−2.000	−4.083	4.177	7.248	6.256	7.799	−1.831	8.521
−2.100	−4.432	4.153	7.209	6.259	7.805	−1.834	8.594
−2.200	−4.786	4.130	7.169	6.261	7.810	−1.837	8.665
−2.300	−5.151	4.106	7.129	6.264	7.814	−1.839	8.735
−2.400	−5.523	4.082	7.089	6.266	7.819	−1.841	8.805
−2.500	−5.908	4.058	7.048	6.268	7.822	−1.843	8.874
−2.600	< −6.00	4.033	7.006	6.270	7.826	−1.845	8.943
−2.700	< −6.00	4.009	6.964	6.272	7.829	−1.846	9.013
−2.800	< −6.00	3.985	6.920	6.274	7.832	−1.848	9.082
−2.900	< −6.00	3.961	6.876	6.275	7.835	−1.849	9.151
−3.000	< −6.00	3.936	6.830	6.277	7.837	−1.850	9.221
−3.100	< −6.00	3.912	6.784	6.278	7.840	−1.852	9.289
−3.200	< −6.00	3.888	6.735	6.280	7.842	−1.853	9.359
−3.300	< −6.00	3.863	6.686	6.281	7.844	−1.854	9.428
−3.400	< −6.00	3.839	6.634	6.282	7.846	−1.855	9.497
−3.500	< −6.00	3.814	6.583	6.283	7.848	−1.856	9.564
−3.600	< −6.00	3.789	6.530	6.284	7.849	−1.856	9.631
−3.700	< −6.00	3.765	6.479	6.284	7.851	−1.857	9.695
−3.800	< −6.00	3.740	6.430	6.285	7.852	−1.858	9.754
−3.900	< −6.00	3.715	6.376	6.286	7.853	−1.858	9.818
−4.000	< −6.00	3.691	6.314	6.286	7.854	−1.859	9.889
−4.100	< −6.00	3.666	6.253	6.287	7.855	−1.859	9.955
−4.200	< −6.00	3.641	6.196	6.287	7.856	−1.860	10.014
−4.300	< −6.00	3.616	6.143	6.288	7.857	−1.860	10.069
−4.400	< −6.00	3.591	6.091	6.288	7.858	−1.861	10.123
−4.500	< −6.00	3.567	6.040	6.288	7.858	−1.861	10.174
−4.600	< −6.00	3.542	5.990	6.289	7.859	−1.861	10.226
−4.700	< −6.00	3.517	5.938	6.289	7.859	−1.861	10.279
−4.800	< −6.00	3.492	5.872	6.289	7.859	−1.861	10.343
−4.900	< −6.00	3.467	5.800	6.289	7.860	−1.862	10.407
−5.0000.....	< −6.00	3.442	5.729	6.289	7.860	−1.862	10.464

massive models, discrepancies between our model radii and the H-S radii are more noticeable and remain significant to much lower temperatures. As expected, the radii and central densities converge to the H-S values as the models cool.

Finally, in Figure 14 we show the luminosity of the models versus their ages. Again, in the WD regime, the results are insensitive to convective efficiency. We remind the reader that the age values corresponding to the early evolution of our models are strongly affected by our choice of zero-age point. In this context, we compare the ages of the 0.25, 0.30, 0.35, and 0.40 $M_\odot$ models at log $(L/L_\odot) = -1$, for which we have log $t = 7.764$, 7.815, 7.805, and 7.780, respectively. At first glance, the 0.30 $M_\odot$ model seems to be the one that takes longer in reaching log $(L/L_\odot) = -1$, but such comparison is not so straightforward. In fact, the 0.35 $M_\odot$ (and not the 0.30 $M_\odot$) initial model is determined by the presence of the forbidden region. Accordingly, we should not compare the ages of the different models at a given luminosity when the ages are comparable to the previous (omitted in this study) evolution. At advanced ages our choice of zero point for the age is no longer significant, and age comparisons between different models is meaningful.

5.2. *Envelope Convection: MLT and CM Models*

As noted in the preceding subsection, the cooling properties of our evolutionary models in the WD regime are practically insensitive to the convection theory employed. By contrast, the structure of the OCZ can be markedly different according to the assumed model of convection. Because the properties of the OCZ of WDs in the MLT have been extensively discussed in the literature (see, e.g., Tassoul et al. 1990, and references therein), we will mainly be concerned with the evolving structure of the OCZ in the CMT. Because this theory has not been widely applied to the study of convective processes in WDs, we believe this topic deserves special attention. In particular, for carbon-oxygen DB WD models, the CMT quite naturally leads to a theo-

TABLE 10

THE HAMADA–SALPETER SEQUENCE FOR $T = 0$ HELIUM WHITE DWARFS

$M/M_\odot$	$\log R/R_\odot$	$\log \rho_c$
0.50.....	−1.864	6.292
0.45.....	−1.842	6.164
0.40.....	−1.817	6.029
0.35.....	−1.792	5.882
0.30.....	−1.764	5.721
0.25.....	−1.734	5.539
0.20.....	−1.699	5.325
0.15.....	−1.657	5.061
0.10.....	−1.602	4.704

retical blue edge in good agreement with observations of pulsating DB WDs (Althaus & Benvenuto 1996). For the sake of completeness, we also include in our study the different versions of the MLT. The results are displayed in Figures 15–20 for He WD models with $M = 0.50$, 0.35, 0.30, 0.15, and 0.10 $M_\odot$. In each figure, we plot the extent of the evolving OCZ in terms of the mass fraction q as a function of $T_{\rm eff}$ for ML3, ML2, ML1, and CM version of convection. In each figure, the location of the photosphere ($\tau = \frac{2}{3}$) almost coincides with the location of the top of the OCZ (which is independent of the model of convection), and it is not shown.

The behavior of the evolving structure of the OCZ during the pre-WD regime can be seen particularly in Figure 18, which corresponds to the 0.3 $M_\odot$ He pre-WD model. During the early (constant luminosity) stages of its evolution, the model is fully convective. As $T_{\rm eff}$ increases, the base of the OCZ retreats steeply toward the surface. This occurs at higher $T_{\rm eff}$ with more efficient convection. At low luminosities, convection is restricted exclusively to a very narrow region located in the outer zone of the model.

As is well known, ionized elements in the outer layers of a WD begin to recombine as a consequence of the decreasing temperatures throughout the outer layers. The corresponding increase in the opacities eventually leads to the onset of

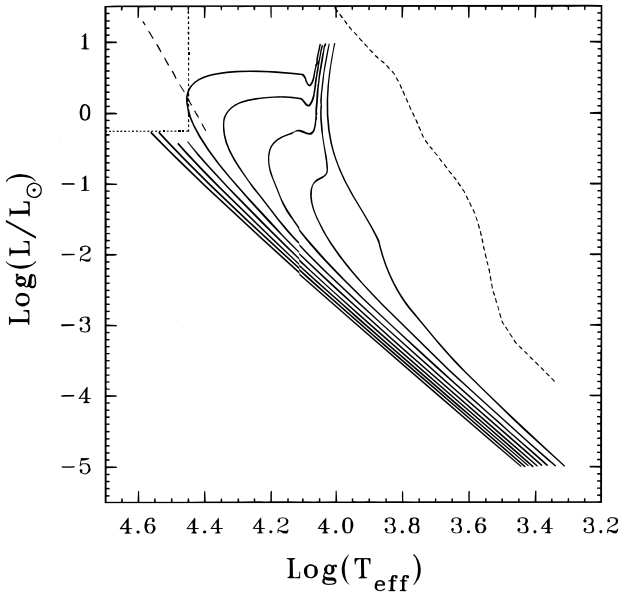

FIG. 1.—Theoretical HR diagram for He WDs according to the CMT. From right to left, He WD models with $M/M_\odot = 0.1$, 0.15, 0.2, 0.25, 0.3, 0.35, 0.4, 0.45, and 0.5 are depicted together with the low-mass, hydrogen-rich main sequence calculated by D'Antona & Mazzitelli (1994) for masses between 0.08 and 2 $M_\odot$. Also, the approximate location of the low-mass helium ZAMS is depicted in long-dashed lines. For an explanation of the apparent contradiction between the evolution of the 0.3 $M_\odot$ WD and the position of the ZAMS, see text. Note the existence of a forbidden region ($\log (L/L_\odot) \geq -0.25$, $\log T_{\rm eff} \geq 4.45$) inside which He WDs can exist only for brief intervals (for more details see text).

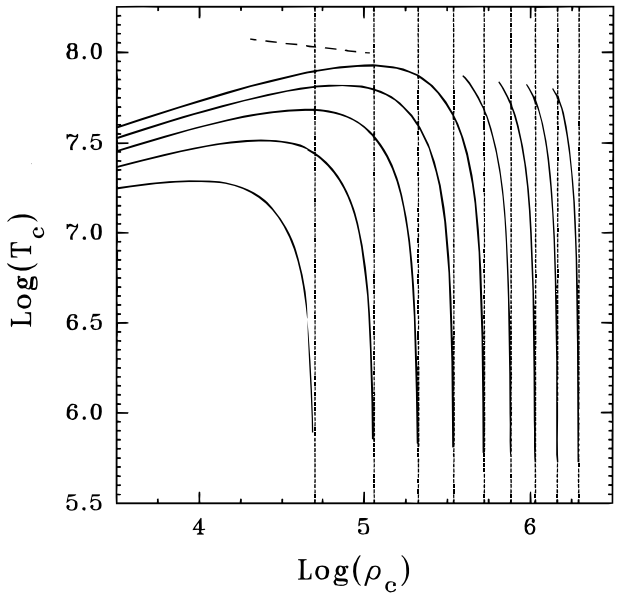

FIG. 2.—Behavior of the central temperature as a function of the central density for our models, from left to right, with $M/M_\odot =$ 0.10, 0.15, 0.20, 0.25, 0.30, 0.35, 0.40, 0.45, and 0.50. Short-dashed straight lines indicate the values of central densities obtained by using the H-S zero-temperature configuration for pure helium. As cooling proceeds, the values of the central density approach the H-S lines, as expected. Also, the approximate location of the low-mass helium ZAMS is depicted in long-dashed lines. Note that, as consequence of neglecting the temporal derivative of the entropy, the ZAMS models are systematically hotter than the calculated employing the full set of stellar evolution equations (for more details, see text).

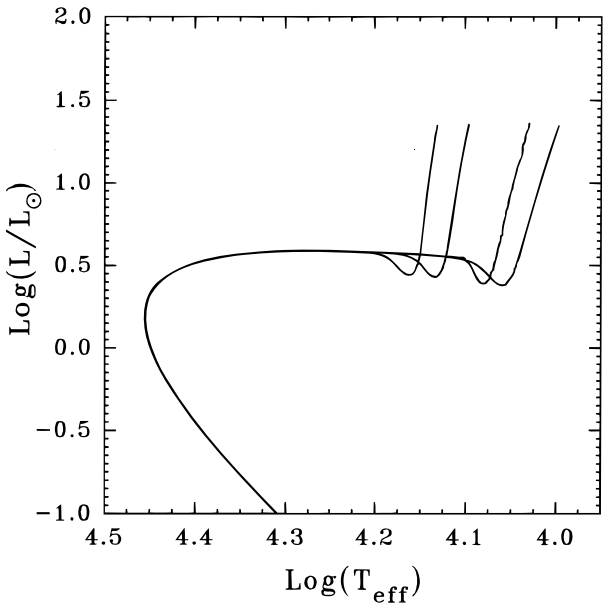

FIG. 3.—Theoretical HR diagram for the 0.3 $M_\odot$ He WD model in the different theories of convection we employed. At high luminosities, from right to left, the results corresponding to ML1, CMT, ML2, and ML3 convection are displayed. Below $\log L/L_\odot = 0.25$, the cooling tracks are insensitive to the treatment of convection.

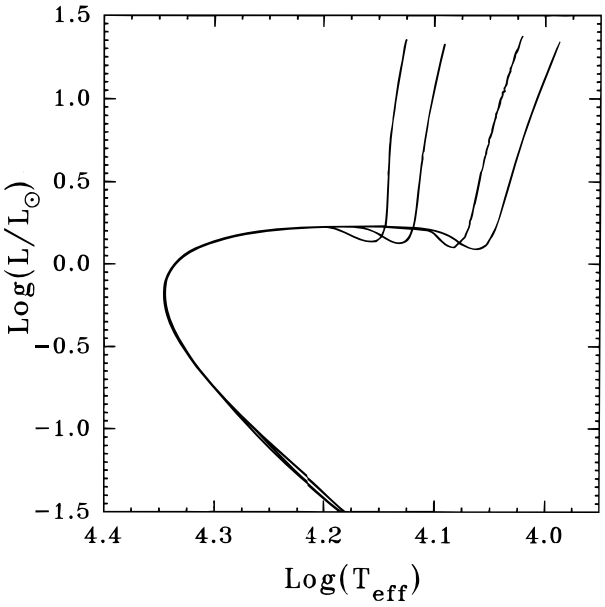

FIG. 4.—Same as Fig. 3 but for the 0.25 $M_\odot$ He WD model

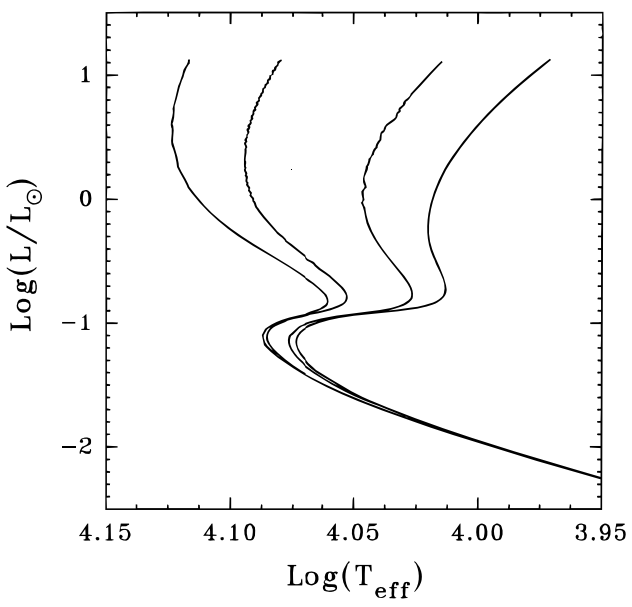

FIG. 6.—Same as Fig. 3 but for the 0.15 $M_\odot$ He WD model

convection, which is also favored by a reduction in the value of ∇_{ad} in partial ionization zones. In the intermediate- and high-luminosity range, the structure of the OCZ depends strongly upon the treatment of convection, as can be noted in Figures 15–18. In the WD regime of our more massive models, the thickness of the OCZ, at a given mass, begins to increase appreciably at higher $T_{\rm eff}$ with more efficient convection. In fact, models with greater convective efficiency are characterized by smaller $\nabla_{\rm conv}$ in the upper part of the envelope. This provides lower temperatures in the deeper layers, resulting in higher opacities, and this is responsible for the deeper convection zone. With further cooling, the high electron conductivity in the upward moving degeneracy boundary causes the base of the convection zone to reach a maximum depth that is independent of the convection theory used, as Figures 15, 16, 17, 19, and 20 show. Note that the location of the base of the convection zone is now determined by the location of the degeneracy boundary. From then on, the different treatments of convection provide an adiabatic stratification for most of the OCZ (a similar result is also obtained by Tassoul et al. 1990). Another trend accounted for by our models is the greater final extent of the OCZ in the less massive, and therefore less degenerate, models (D'Antona & Mazzitelli 1979).

The evolving structure of the OCZ in the CMT is markedly different from that given by any version of the MLT. The resulting convective profile cannot be reproduced by any choice of the MLT free parameters. This behavior results essentially from the interplay between the higher values of $\Phi^{\rm CM}$ (respect to that of the MLT) for large Σ and the small values of z in the outer layers. If we analyze the behavior of the evolving OCZ of our 0.5 $M_\odot$ model in Figure 15, the extent of the OCZ is almost the same at high $T_{\rm eff}$, independent of the convective efficiency. In this case, convection contributes negligibly to the energy transport. As $T_{\rm eff}$ decreases, the more efficient convection (larger con-

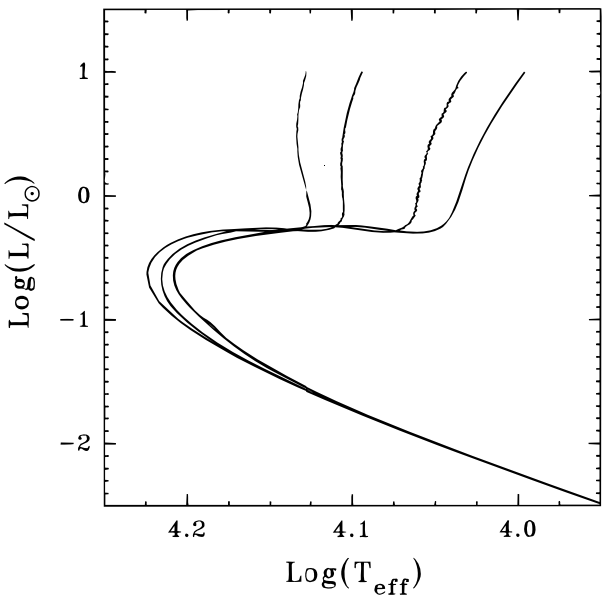

FIG. 5.—Same as Fig. 3 but for the 0.20 $M_\odot$ He WD model

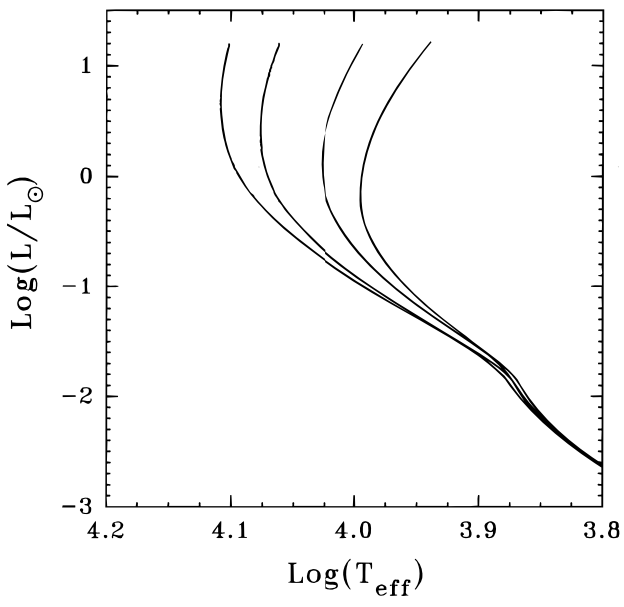

FIG. 7.—Same as Fig. 3 but for the 0.10 $M_\odot$ He WD model

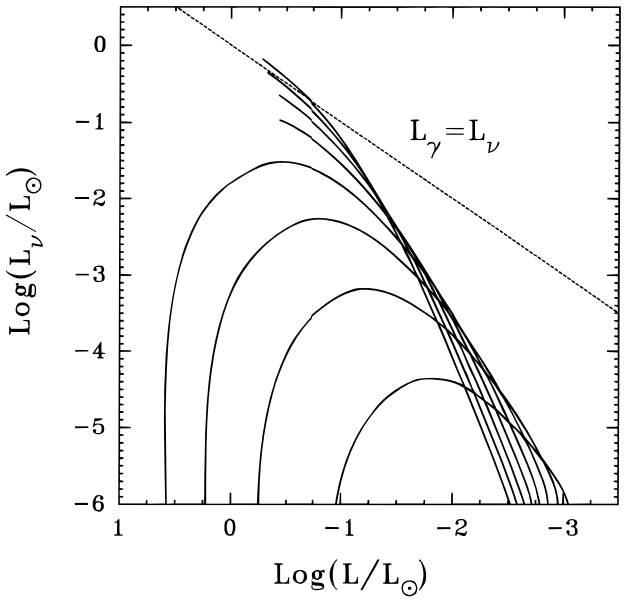

FIG. 8.—Neutrino luminosity (in solar units) vs. stellar luminosity corresponding to He WD models with (*from top to bottom*) $M/M_\odot$ = 0.5, 0.45, 0.4, 0.35, 0.3, 0.25, 0.2, and 0.15. For the sake of reference, the line $L_\gamma = L_\nu$ is also shown. It is obvious that neutrino energy losses should be considered for the more massive models during their high-temperature phases.

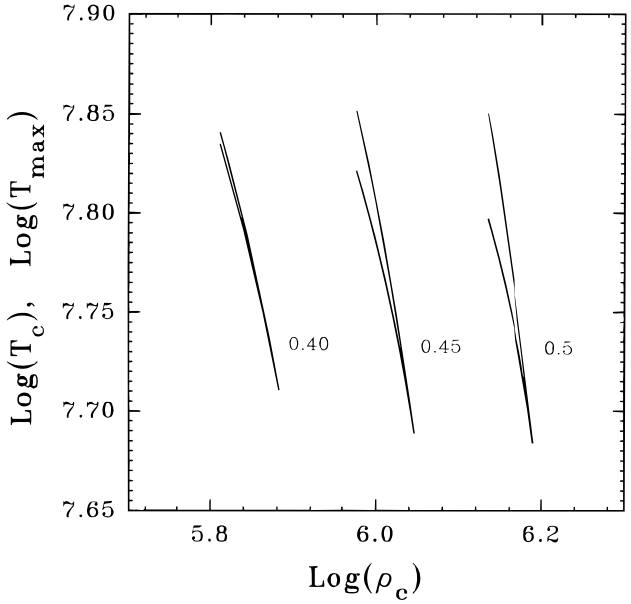

FIG. 10.—Central and maximum temperatures vs. central density for 0.5, 0.45, and 0.4 $M_\odot$ He WD models (for each mass, the right-hand curve corresponds to the maximum temperature). At high-luminosity phases, neutrino losses lead to maximum temperatures appreciably different from the central temperature, notably for more massive models. For lower masses or somewhat lower luminosities, the maximum temperature occurs at the center of the model.

vective flux) of CMT compared to ML1 makes the OCZ of the CMT model deeper. With further cooling, most of the OCZ becomes adiabatic in both theories, and any difference in the temperature stratification is due primarily to the behavior of ∇_{conv} (which, in the CMT, is now governed by the small eddy size) in the thin region close to the stellar surface. Finally, at sufficiently low luminosities, almost all the OCZ assumes an adiabatic stratification and the extent of the OCZ becomes insensitive to the treatment of convection. For the case of He WDs in the range of masses of 0.4–0.5 $M_\odot$, the present results strongly resemble those presented in Althaus & Benvenuto (1996) for the case of carbon-oxygen DB WDs.

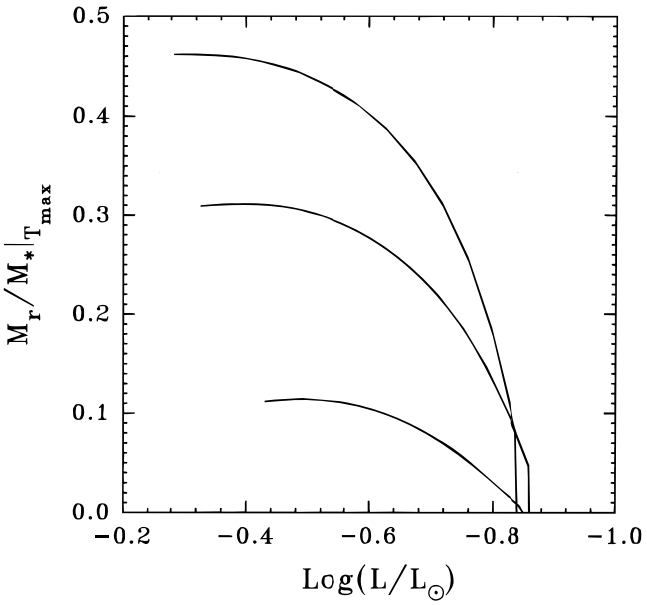

FIG. 9.—The location of the maximum temperature in the Lagrangian coordinate vs. stellar luminosity for (*from top to bottom*) 0.5, 0.45, and 0.4 $M_\odot$ He WD models. For the other masses, the maximum temperature occurs in the center throughout the entire evolution.

6. CONCLUSIONS

In this study, we present detailed calculations of low-mass, helium white dwarf (He WD) models with masses from $M = 0.1\ M_\odot$ to $M = 0.5\ M_\odot$ at intervals of $0.05\ M_\odot$ and a metallicity of $Z = 10^{-3}$. To this end, we take into

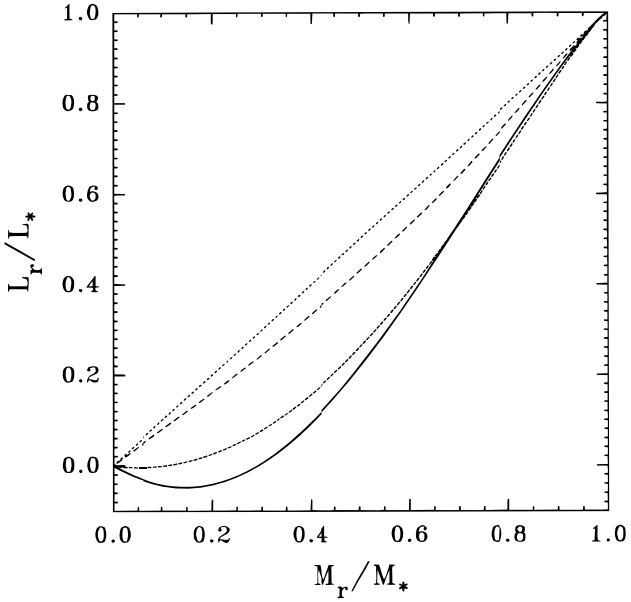

FIG. 11.—Fractional luminosity vs. the mass fraction for the model of 0.45 $M_\odot$ at log T_{eff} = 4.54, 4.42, and 4.34 corresponding to the solid line, short-dashed line, and long-dashed line, respectively. As a result of neutrino emission, the luminosity is not proportional to the mass in the WD interior for hot models. As the models cool down, they come closer to satisfying the proportionality relation (*dotted line*).

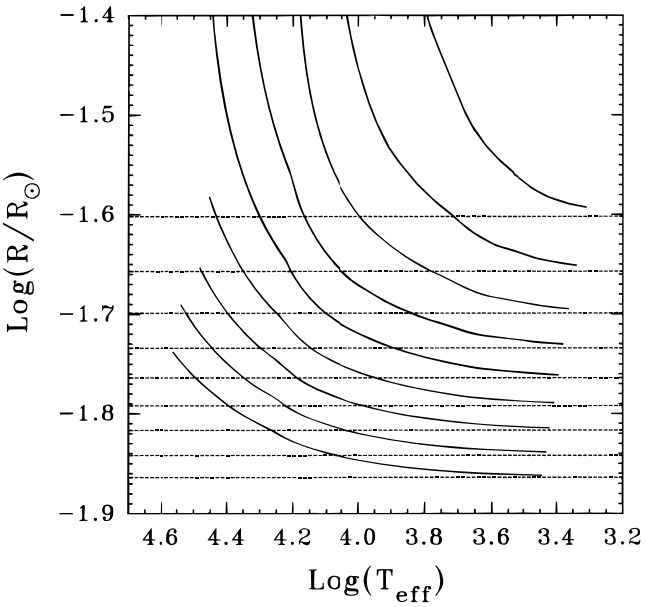

FIG. 12.—Radii (in solar units) vs. $T_{\rm eff}$ for models (*from bottom to top*) with $M/M_\odot$ = 0.50, 0.45, 0.40, 0.35, 0.30, 0.25, 0.20, 0.15, and 0.10 according to the CMT. Short-dashed straight lines indicate values obtained by using the H-S zero-temperature configuration for pure helium. Finite-temperature effects are noticeable, particularly for less massive models.

account finite-temperature effects by means of a detailed and updated stellar evolutionary code in which the convective energy transport is described according to the new model for turbulent convection developed by Canuto & Mazzitelli (1991, 1992). Furthermore, our code uses the most recent opacity data computed by the Livermore Group (OPAL data; Rogers & Iglesias 1994), and also the new equation of state for helium plasmas developed by Saumon et al. (1995). Neutrino emission is fully taken into account as well.

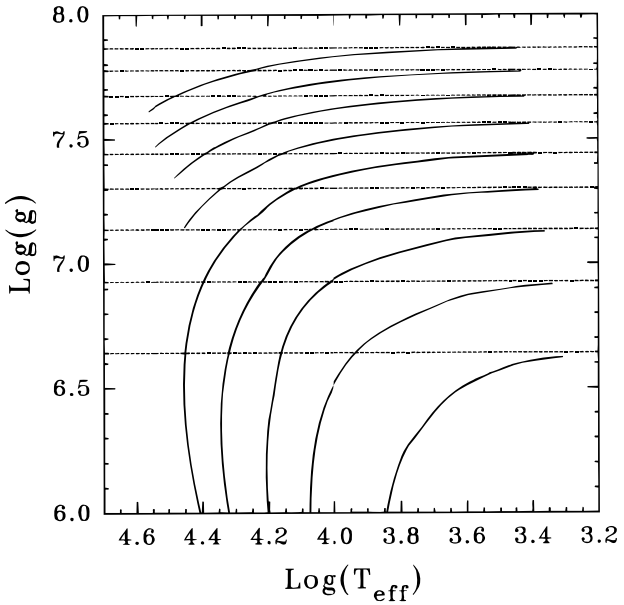

FIG. 13.—Surface gravities vs. $T_{\rm eff}$ for models (*from top to bottom*) with $M/M_\odot$ = 0.5, 0.45, 0.4, 0.35, 0.3, 0.25, 0.2, 0.15, and 0.1 according to the CMT. Short-dashed straight lines indicate values obtained by using the H-S zero-temperature configuration for pure helium. Again, finite-temperature effects are noticeable for the less massive models.

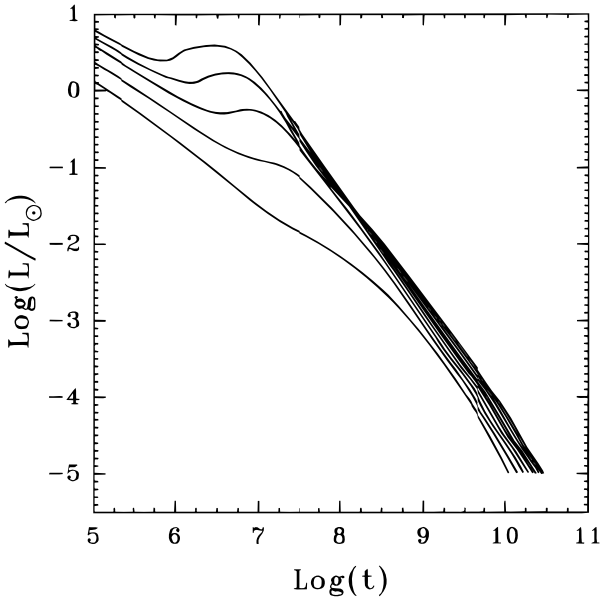

FIG. 14.—Age (in yr) vs. luminosity relation for models (*from top to bottom*) with $M/M_\odot$ = 0.50, 0.45, 0.40, 0.35, 0.30, 0.25, 0.20, 0.15, and 0.10. For the choice of the time origin and its importance, see text.

The present calculations represent the most extensive study of low-mass He WDs to date, and we believe these models will be useful for future investigations concerning the interpretation of observations of these stars.

We pick starter models that will yield accurate evolutionary models in the WD cooling regime. For models with $M \leq 0.3\ M_\odot$, we started our calculations from fully convective models located near the helium-Hayashi line for each configuration, far away from the WD regime. By contrast, the evolutionary sequences corresponding to 0.35, 0.40, 0.45, and 0.50 $M_\odot$ were started from initial models resembling WD structures. This is necessary if we want to avoid

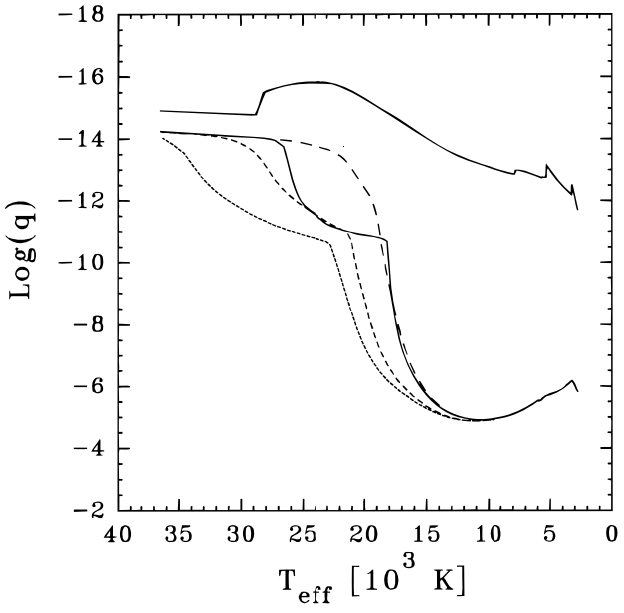

FIG. 15.—Extent of the OCZ for the 0.5 $M_\odot$ He WD model. The location of the top and the base of the OCZ is expressed in terms of the mass fraction q as a function of $T_{\rm eff}$ for the cases ML3 (*dotted line*), ML2 (*short-dashed line*), ML1 (*long-dashed line*), and CM (*solid line*) convective models. The top of the OCZ is the same for all the convection treatments employed here. Evolution is from left to right.

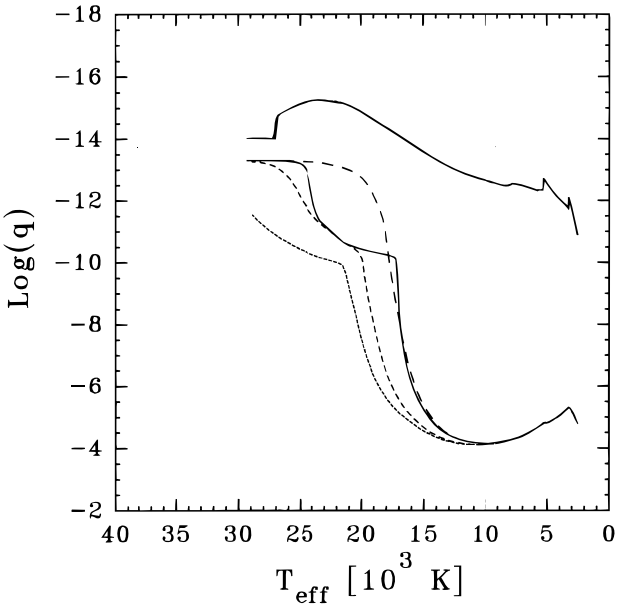

FIG. 16.—Same as in Fig. 15, but for the 0.35 $M_\odot$ He WD model

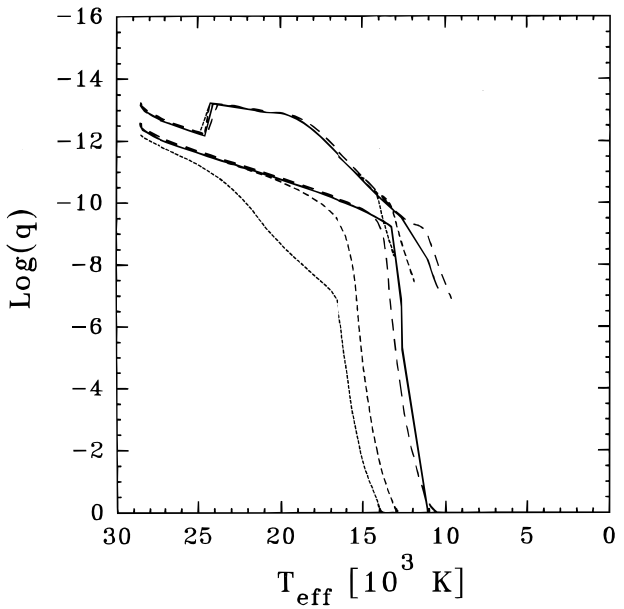

FIG. 18.—Same as in Fig. 17, but for the pre-WD regime. Note that in the early stages of its evolution, the model is fully convective. As T_{eff} increases, the base of the OCZ retreats toward the surface of the model. Evolution is from right to left.

the onset of core helium burning. Because of this requirement, we found a "forbidden region" in the HR diagram where He WDs can exist only for brief intervals. This region covers $\log (L/L_\odot) \geq -0.25$ and $\log T_{eff} \geq 4.45$. In this context, all of our evolutionary tracks should be asymptotically reached by helium objects resulting from the binary evolution. All the models were evolved down to $\log (L/L_\odot) = -5$. At the lowest luminosities, our models are less reliable because they require extrapolations of physical quantities, such as the radiative opacities.

The evolutionary tracks in the HR diagram have been carefully analyzed, and we find that the convective efficiency affects them noticeably only in the high-luminosity (pre-WD) regime. We also examined the evolution of central conditions, neutrino luminosity, radii, surface gravities, and ages. We found that neutrino losses considerably affect both the cooling and structural properties of He WD configurations above 0.35 $M_\odot$ and therefore must be included. Regarding the central temperature, radius, and surface gravity evolution, we find that our He WD models start out at up to twice the Hamada & Salpeter (1961) radius due to

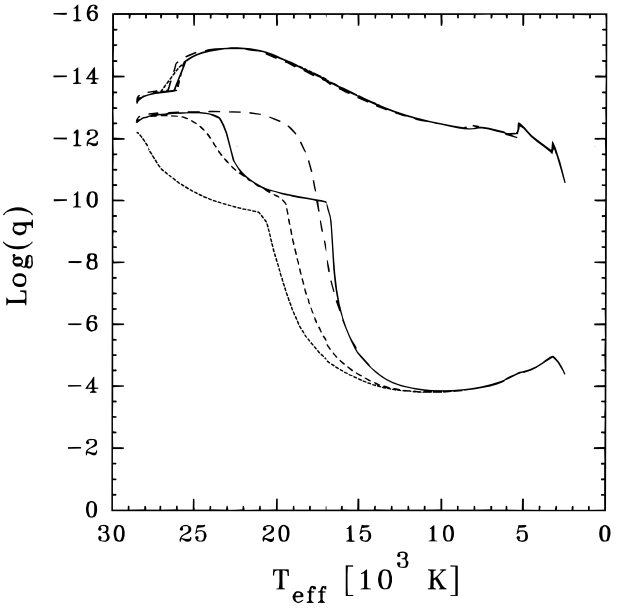

FIG. 17.—Same as in Fig. 15, but for the 0.3 $M_\odot$ He model in the WD regime.

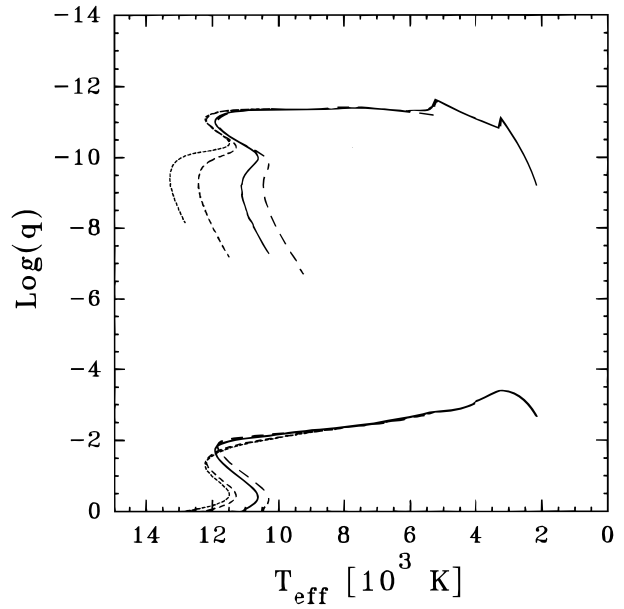

FIG. 19.—Extent of the OCZ for the 0.15 $M_\odot$ model. The meaning of the lines is the same as in Fig. 15. In the early (pre-WD) stages of evolution, the model is fully convective. In the WD regime, the OCZ is thicker than in more massive models. This is due to the less degree of degeneracy characterizing the less massive models. Thus, conductive opacity plays a minor role and the presence of convection is favored. The location of the photosphere remains very deep during the entire evolution of the model. This is due to the very low helium opacities at low densities and temperatures, which leads to very transparent atmospheres. The kink in the location of top of the OCZ with decreasing T_{eff} is due to the fact that the two sets of radiative opacities employed in our study do not overlap smoothly.

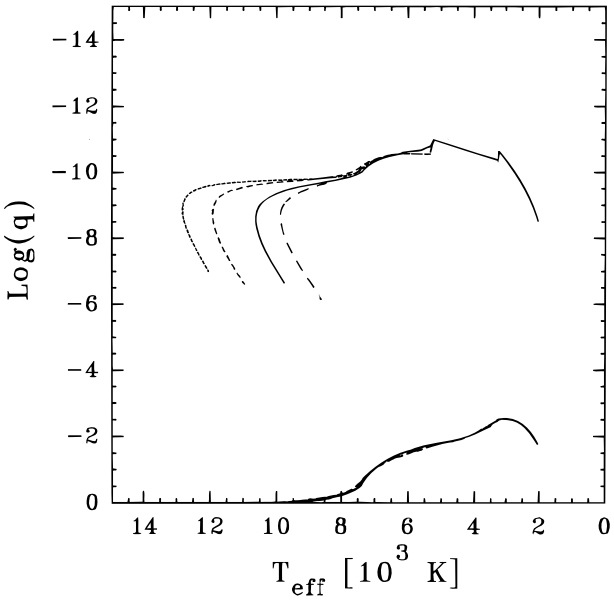

FIG. 20.—Same as in Fig. 19, but for the 0.10 $M_\odot$ He WD model

finite-temperature effects. As cooling proceeds, the models asymptotically approach the zero temperature Hamada & Salpeter (1961) results, as expected.

Finally, the structure of the evolving outer convection zone was analyzed in both the framework of the mixing length theory (for different convective efficiencies) and the CM theory. We found that the profile of the outer convection zone given by the CM theory is markedly different from that given by any version of the mixing length theory. Although this behavior is critical for pulsational instability, it does not significantly affect stellar parameters such as radius and surface gravity in the WD domain.

In a future work we shall apply these results to the analysis of the presently known low-mass WDs. More detailed tabulations of our results are available upon request to the authors at their e-mail address.

We are deeply indebted to Francesca D'Antona for sending us the starting model, Italo Mazzitelli for his EOS, and to Forrest Rogers for providing us with his radiative opacity data tables. Also, we deeply acknowledge Tristan Guillot and Didier Saumon for their help in making available to us the low- and intermediate-density EOS we employed here. It is a pleasure to thank our referee, Paul A. Bradley, for his exhaustive reports, which made it possible to improve significantly the original version of this work. We also grateful to Icko Iben, Jr., for providing us with material before its publication. Finally, we acknowledge Rodolfo Barbá for helping us with the TeX.

This work has been partially supported by the Comisión de Investigaciones Científicas de la Provincia de Buenos Aires, the Consejo Nacional de Investigaciones Científicas y Técnicas (Argentina) through the Programa de Fotometría y Estructura Galáctica (PROFOEG), and the University of La Plata.

APPENDIX

THE THOMAS-FERMI AND EXCHANGE CONTRIBUTIONS FOR STRONG DEGENERACY

The free energy for the Thomas-Fermi correction at finite temperature was taken from Shaviv & Kovetz (1972) (in the expression given by these authors a $4\pi/3$ factor is missing)

$$F_{\rm TF} = -\frac{2\pi}{3} e^2 N_i k_{\rm B} T \langle r\rangle^2 g(\Gamma) \frac{\partial n_e}{\partial \mu}\,, \tag{A1}$$

where e stands for the electron charge, N_i is number of ions, n_e is the electron number density, $k_{\rm B}$ is Boltzmann's constant, and μ is the chemical potential. The quantity $\langle r\rangle$ is related to the ion number density n_i through $4\pi\langle r\rangle^3/3 = n_i^{-1}$ and $g(\Gamma)$ is given by $g(\Gamma) = 0.6175\Gamma$, where Γ is the plasma coupling constant defined by $\Gamma = (Z^2e^2)/(\langle r\rangle KT)$.

In order to derive the thermodynamic quantities of interest, we have rewritten the free energy as

$$F_{\rm TF} = -\frac{162}{175}\left(\frac{4}{9\pi}\right)^{2/3} \alpha^2 mc^2 Z^{4/3}(F_0 + \gamma^2 F_2 + \gamma^4 F_4)\,, \tag{A2}$$

where $F_{\rm TF}$ is the free energy *per electron*, m is the electron mass, α is the fine structure constant, $\gamma = k_{\rm B}T/mc^2$, and

$$F_0 = \sqrt{x^2+1}\,, \tag{A3}$$

$$F_2 = -\frac{\pi^2}{3}\frac{\sqrt{x^2+1}}{x^4}\,, \tag{A4}$$

$$F_4 = \pi^4\sqrt{x^2+1}\left(\frac{1}{9}\frac{x^2+2}{x^6} - \frac{4}{15}\frac{1}{x^8}\right), \tag{A5}$$

where x is the dimensionless Fermi momentum given by $x^2 = (\mu/mc^2)^2 - 1$. From the foregoing equations we obtain for the internal energy per electron $E_{\rm TF}$,

$$E_{\rm TF} = -\frac{162}{175}\left(\frac{4}{9\pi}\right)^{2/3} \alpha^2 mc^2 Z^{4/3}(E_0 + \gamma^2 E_2 + \gamma^4 E_4)\,, \tag{A6}$$

with $E_0 = F_0$ and

$$E_2 = \frac{\pi^2}{3}\frac{1}{x^4\sqrt{x^2+1}}(2x^4+2x^2+1)\,, \tag{A7}$$

$$E_4 = \frac{\pi^4}{45x^8\sqrt{x^2+1}}(-25x^6-15x^4+74x^2+56)\,, \tag{A8}$$

and for the pressure

$$P_{\rm TF} = -mc^2\left(\frac{mc}{\hbar}\right)^3\frac{162}{175}\left(\frac{4}{9\pi}\right)^{2/3}\frac{\alpha^2}{3\pi^2}Z^{4/3}(P_0+\gamma^2P_2+\gamma^4P_4)\,, \tag{A9}$$

where

$$P_0 = \frac{1}{3}\frac{x^5}{\sqrt{x^2+1}}\,, \tag{A10}$$

$$P_2 = \frac{\pi^2}{18x\sqrt{x^2+1}}(10x^4+13x^2+8)\,, \tag{A11}$$

$$P_4 = \frac{\pi^4}{270x^5\sqrt{x^2+1}}\left(10x^6+90x^4+\frac{1803}{4}x^2-52\right). \tag{A12}$$

Note that as $T \to 0$ these expressions tend to those given by Salpeter (1961).

The exchange contribution to the free energy at finite temperature F_E is given by Kovetz et al. (1972) and Shaviv & Kovetz (1972). Here we considered the free energy and not the thermodynamic potential as it is assumed by the authors; otherwise neither the nonrelativistic nor the $T = 0$ limits are correctly obtained. F_E is given by

$$F_E = \frac{\alpha}{4\pi^3}mc^2\left(\frac{mc}{\hbar}\right)^3V[F_0(x)+\gamma^2F_2(x,\,T)+\gamma^4F_4(x)]\,, \tag{A13}$$

where $\beta = x + (1+x^2)^{1/2}$ and

$$F_0(x) = \tfrac{1}{32}(\beta^4+\beta^{-4}) + \tfrac{1}{4}(\beta^2+\beta^{-2}) - \tfrac{9}{16} - \tfrac{3}{4}(\beta^2-\beta^{-2})\ln\beta + \tfrac{3}{2}(\ln\beta)^2\,, \tag{A14}$$

$$F_2(x,\,T) = 4(g_2-2g_1) + \frac{\pi^2}{3}\left(1+x^2+2\ln\frac{2x^2}{\gamma} - \frac{3\sqrt{x^2+1}}{x}\ln\beta\right), \tag{A15}$$

$$F_4(x) = -\frac{7\pi^4}{60}(x^{-2}+2x^{-4}+3\sqrt{x^2+1}x^{-5}\ln\beta) + \frac{\pi^4}{36}(2+2x^{-2}+x^{-4})\,. \tag{A16}$$

The values of g_2 and g_1 are 0.449 and -0.504, respectively. The corresponding internal energy can be written as

$$E_E = \frac{\alpha}{4\pi^3}mc^2\left(\frac{mc}{\hbar}\right)^3V[E_0(x)-\gamma^2E_2(x,\,T)-\gamma^4E_4(x)]\,, \tag{A17}$$

with $E_0(x) = F_0(x)$ and

$$E_2(x,\,T) = 4(g_2-2g_1) + \frac{\pi^2}{3}\left[1-3x^2+2\ln\frac{2x^2}{\gamma} + \frac{3(3x^2+1)}{x\sqrt{x^2+1}}\ln\beta\right], \tag{A18}$$

$$E_4(x) = -\frac{\pi^4}{x^4}\left[\frac{1}{60x\sqrt{x^2+1}}(80x^4+103x^2-21)\ln\beta + \frac{1}{180}(-30x^4+113x^2+235)\right], \tag{A19}$$

and for the pressure

$$P_E = \frac{\alpha}{4\pi^3}mc^2\left(\frac{mc}{\hbar}\right)^3[P_0(x)+\gamma^2P_2(x,\,T)+\gamma^4P_4(x)]\,, \tag{A20}$$

where

$$P_0(x) = \frac{1}{6}(x^2-9)x^2 + \frac{x(x^2+3)}{\sqrt{x^2+1}}\ln\beta - \frac{3}{2}\ln^2\beta\,, \tag{A21}$$

$$P_2(x, T) = -4(g_2 - 2g_1) - \frac{\pi^2}{3}\left(-\frac{2}{3} - x^2 + 2\ln\frac{2x^2}{\gamma} + \frac{x}{\sqrt{x^2+1}}\ln\beta\right), \quad \text{(A22)}$$

$$P_4(x) = \frac{4}{9}\frac{\pi^4}{x^5}\left[-\frac{1}{8}x^5 + \frac{9}{16}x^3 + \frac{37}{20}x + \frac{x^2}{\sqrt{x^2+1}}\left(x^2 + \frac{227}{80}\right)\ln\beta\right]. \quad \text{(A23)}$$

Again, the results given by Salpeter (1961) are obtained when in our equations $T \to 0$.

REFERENCES

Althaus, L. G., & Benvenuto, O. G. 1996, MNRAS, 278, 981
Benvenuto, O. G. 1988, Ph.D. thesis, Univ. Nacional de La Plata
Benvenuto, O. G., & Althaus, L. G. 1995, Ap&SS, 234, 11
Bergeron, P., Saffer, R. A., & Liebert, J. 1992, ApJ, 394, 228
Böhm-Vitense, E. 1958, Z. Astrophys., 46, 108
Bradley, P. A., & Winget, D. E. 1994, ApJ, 421, 236
Bragaglia, A., Renzini, A., & Bergeron, P. 1995, ApJ, 443, 735
Canuto, V. M., & Mazzitelli, I. 1991, ApJ, 370, 295
———. 1992, ApJ, 389, 724
Chandrasekhar, S. 1939, An Introduction to the Study of Stellar Structure (Chicago: Univ. Chicago Press)
Chin, C.-W., & Stothers, R. B. 1971, ApJ, 163, 555
Cox, A. N., & Stewart, J. 1970, ApJS, 19, 261
Cox, J. P., & Giuli, R. T. 1968, Principles of Stellar Structure, Vol. 1 (New York: Gordon & Breach)
D'Antona, F., Magni, G., & Mazzitelli, I. 1972, Ap&SS, 19, 151
D'Antona, F., & Mazzitelli, I. 1979, A&A, 74, 161
———. 1990, ARA&A, 28, 139
———. 1994, ApJS, 90, 467
D'Antona, F., Mazzitelli, I., & Gratton, R. G. 1992, A&A, 257, 539
de Kool, M., & Ritter, H. 1993, A&A, 267, 397
Fontaine, G., & Van Horn, H. M. 1976, ApJS, 31, 467
Fontaine, G., & Wesemael, F. 1991, in IAU Symp. 145, Evolution of Stars: the Photospheric Abundance Connection, ed. G. Michaud & A. V. Tutukov (Dordrecht: Kluwer), 421
Hamada, T., & Salpeter, E. E. 1961, ApJ, 134, 683
Hansen, J. P. 1973, Phys. Rev. A, 8, 3096
Hubbard, W. B., & Lampe, M. 1969, ApJS, 18, 297
Huebner, W. F., Merts, A. L., Magee, N. H., Jr., & Argo, M. F. 1977, Rep. LA-6760 (Los Alamos: Los Alamos Nat. Lab.)
Iben, I., Jr., & Tutukov, A. V. 1993, ApJ, 418, 343
Iben, I., Jr., Tutukov, A. V., & Yungelson, L. R. 1996, ApJ, 475, in press
Iben, I., Jr., & Webbink, R. F. 1989, in IAU Colloq. 114, White Dwarfs, ed. G. Wegner (Berlin: Springer), 477
Iglesias, C. A., & Rogers, F. J. 1993, ApJ, 412, 752
Itoh, N., & Kohyama, Y. 1983, ApJ, 275, 858
Itoh, N., Adachi, T., Nakagawa, M., Kohyama, Y., & Munakata, H. 1989, ApJ, 339, 354; erratum 360, 741 (1990)
Itoh, N., Mitake, S., Iyetomi, H., & Ichimaru, S. 1983, ApJ, 273, 774
Itoh, N., Mutoh, H., Hikita, A., & Kohyama, Y. 1992, ApJ, 395, 622; erratum 404, 418 (1993)
Kippenhahn, R., & Thomas, H. 1964, ZAp 60, 19
Kippenhahn, R., & Weigert, A. 1990, Stellar Structure and Evolution (Berlin: Springer)
Kippenhahn, R., Weigert, A., & Hofmeister, E. 1967, in Methods in Computational Physics 7, ed. B. Alder, S. Fernbach, & M. Rottenberg (New York: Academic Press), 129
Koester, D., Allard, N. F., & Vauclair, G. 1994, A&A, 291, L9
Koester, D., & Schönberner, D. 1986, A&A, 154, 125
Kovetz, A., Lamb, D. Q., & Van Horn, H. M. 1972, ApJ, 174, 109
Lundgren, S. C., Cordes, J. M., Foster, R. S., Wolszczan, A., & Camilo, F. 1996, ApJ, 458, L33
Magni, G., & Mazzitelli, I. 1979, A&A, 72, 134
Marsh, T. R. 1995, MNRAS, 275, L1
Marsh, T. R., Dhillon, V. S., & Duck, S. R. 1995, MNRAS, 275, 828
Marsh, T. R., & Duck, S. R. 1996, MNRAS, 278, 565
Mazzitelli, I. 1993, private communication
———. 1994, private communication
Mazzitelli, I., & D'Antona, F. 1991, in Seventh European Workshop on White Dwarfs, ed. G. Vauclair & E. M. Sion (Dordrecht: Kluwer), 305
Mihalas, D. 1970, Stellar Atmospheres (San Francisco: Freeman)
Munakata, H., Kohyama, Y., & Itoh, N. 1987, ApJ, 316, 708
Nelson, L. A., Joss, P. C., & Rappaport, S. 1989, in IAU Colloq. 114, White Dwarfs, ed. G. Wegner (Berlin: Springer), 469
Paternò, L., Ventura, R., Canuto, V. M., & Mazzitelli, I. 1993, ApJ, 402, 733
Rogers, F. J., & Iglesias, C. A. 1994, Science, 263, 50
Salpeter, E. E. 1961, ApJ, 134, 669
Saumon, D., Chabrier, G., & Van Horn, H. M. 1995, ApJS, 99, 713
Shaviv, G., & Kovetz, A. 1972, A&A, 16, 72
Stothers, R. B., & Chin, C.-W. 1995, ApJ, 440, 297
Tassoul, M., Fontaine, G., & Winget, D. E. 1990, ApJS, 72, 335
Thejll, P., Vennes, S., & Shipman, H. L. 1991, ApJ, 370, 355
Van Horn, H. M. 1968, ApJ, 151, 227
Vennes, S., Fontaine, G., & Brassard, P. 1995, A&A, 296, 117
Vennes, S., & Thorstensen, J. R. 1994, AJ, 108, 1881
Wallace, R. K., Woosley, S. E., & Weaver, T. A. 1982, ApJ, 258, 696
Winget, D. E., Van Horn, H. M., Tassoul, M., Hansen, C. J., & Fontaine, G. 1983, ApJ, 268, L33
Winget, D. E., Van Horn, H. M., Tassoul, M., Hansen, C. J., Fontaine, G., & Carroll, B. W. 1982, ApJ, 252, L65